

2019-06-06

Linking direct measurements of turbidity currents to submarine canyon-floor deposits

Maier, K

<http://hdl.handle.net/10026.1/14197>

10.3389/feart.2019.00144

Frontiers in Earth Science

Frontiers Media

All content in PEARL is protected by copyright law. Author manuscripts are made available in accordance with publisher policies. Please cite only the published version using the details provided on the item record or document. In the absence of an open licence (e.g. Creative Commons), permissions for further reuse of content should be sought from the publisher or author.

Linking direct measurements of turbidity currents to submarine canyon-floor deposits

1 **Running Title:** Linking Flow Measurements with Turbidites

2 **Katherine L. Maier^{1,2*}, Jennifer Gales³, Charles K. Paull¹, Kurt Rosenberger², Peter J.**
3 **Talling⁴, Stephen M. Simmons⁵, Roberto Gwiazda¹, Mary McGann⁶, Matthieu J. Cartigny⁴,**
4 **Eve Lundsten¹, Krystle Anderson¹, Michel A. Clare⁷, Jingping Xu⁸, Daniel Parsons⁵, James P.**
5 **Barry¹, Monica Wolfson-Schwehr¹, Nora M. Nieminski⁹, Esther J. Sumner¹⁰, and the Monterey**
6 **Coordinated Canyon Experiment Team**

7 ¹Monterey Bay Aquarium Research Institute, Moss Landing, California, USA

8 ²Pacific Coastal and Marine Science Center, U.S. Geological Survey, Santa Cruz, California, USA

9 ³School of Biological and Marine Sciences, University of Plymouth, Plymouth, Devon, UK

10 ⁴Departments of Geography and Earth Sciences, University of Durham, Durham, UK

11 ⁵Energy and Environment Institute, University of Hull, Hull, UK

12 ⁶Pacific Coastal and Marine Science Center, U.S. Geological Survey, Menlo Park, California, USA

13 ⁷National Oceanography Centre, University of Southampton, Southampton, UK

14 ⁸Southern University of Science and Technology of China, Shenzhen, Guangdong, China

15 ⁹Department of Geological Sciences, Stanford University, Stanford, CA, USA

16 ¹⁰School of Ocean and Earth Science, University of Southampton, Southampton, UK

17 *** Correspondence:**

18 Dr. Katherine L. Maier

19 Katie.Maier@niwa.co.nz; present affiliation: National Institute of Water and Atmospheric Research,
20 Wellington, New Zealand

21 **Keywords: submarine canyon, sediment density flow, turbidity current, turbidite, sediment**
22 **trap, Monterey Canyon**

23 **Abstract**

24 Submarine canyons are conduits for episodic and powerful sediment density flows (commonly called
25 turbidity currents) that move globally significant amounts of terrestrial sediment and organic carbon
26 into the deep sea, forming some of the largest sedimentary deposits on Earth. The only record
27 available for most turbidity currents is the deposit they leave behind. Therefore, to understand
28 turbidity current processes, we need to determine the degree to which these flows are represented by
29 their deposits. However, linking flows and deposits is a major long-standing scientific challenge.
30 There are few detailed measurements from submarine turbidity currents in action, and even fewer
31 direct measurements that can be compared to resulting seabed deposits. Recently, an extensive array
32 of moorings along Monterey Canyon, offshore California, took measurements and samples during
33 sediment density flow events, providing the most comprehensive dataset to date of turbidity current
34 flows and their deposits. Here, we use sediment trap samples, velocity measurements, and seafloor

35 cores to document how sand is transported through a submarine canyon, and how the transported
 36 sediment is represented in seafloor deposits. Sediment trap samples from events contain primarily
 37 fine to medium-grained sand with sharp bases, normal grading, and muddy tops. Sediment captured
 38 from the water column during the flow shows normal grading, which is broadly consistent with the
 39 initial peak and waning of flow velocities measured at a single height within the flow, and may be
 40 enhanced by collapsing flows. Flow events contain coarser sand concentrated toward the seafloor and
 41 larger grain sizes on the seafloor or in the dense near-bed layer, possibly representative of stratified
 42 flows. Although flow velocity varies, sand grain sizes in sediment traps are similar over distances of
 43 50 km down-canyon, suggesting that grain size is an unfaithful record of down-canyon changes in
 44 maximum flow speeds. Sand transported within flow events and sampled in sediment traps is similar
 45 to sand sampled from the seafloor shortly after the events, but traps do not contain pebbles and gravel
 46 common in seabed deposits. Seabed deposits thus appear to faithfully record the sand component that
 47 is transported in the water column during sub-annual turbidity currents.

48

49 **1 Introduction**

50 The stratigraphic record is the primary archive from which Earth's history is deciphered. Persistent
 51 challenges in sampling directly from sediment-laden flows in many environments, and subsequently
 52 sampling their deposits, have resulted in continued debate regarding the fidelity to which sedimentary
 53 deposits record sediment transport processes (e.g., Hodgson et al., 2018). Modern sediment transport
 54 processes in the deep sea have been especially difficult to observe, measure, and sample in submarine
 55 canyon environments (e.g., Paull et al., 2010, 2018; Talling et al., 2015) because of great water
 56 depths, and the often-unpredictable timing, and destructive potential of some powerful flows (e.g.,
 57 Harris and Whiteway, 2011; Xu, 2011; Xu et al., 2014; Clare et al., 2017). Turbid mixtures of
 58 sediment and seawater are driven down submarine canyons by density differences between the flow
 59 and surrounding seawater. These mixtures, termed sediment density flows (and commonly referred to
 60 as turbidity currents), are responsible for the offshore transport of large amounts of sediment into the
 61 deep sea and accumulation of submarine fans (e.g., Talling et al., 2015). Decades of research have
 62 recognized, mapped, and sampled sediment density flow deposits (e.g., turbidites) (e.g., Shepard,
 63 1951; Normark, 1974; Mutti and Normark, 1987; Cronin and Kidd, 1998; Williams et al., 1998;
 64 Anderson et al., 2006) without the benefit of comprehensive observations of modern processes. In a
 65 small number of submarine canyons, sediment traps have been successfully deployed to capture
 66 sediment directly from within turbidity currents (e.g., Xu et al., 2010, 2014; Liu et al., 2016).
 67 However, there are very few examples of comparisons between direct flow measurements and
 68 resulting seabed deposits (e.g., Symons et al., 2017; Hage et al., 2018). This study provides the most
 69 detailed comparison to date between measured sediment density flows (Paull et al., 2018) paired with
 70 samples of suspended sediment and resulting seabed deposits. Thus, this dataset allows us to address
 71 how sediment density flows are recorded by deposits, and the fidelity of that record.

72 In recent years, advances in technology have allowed turbidity currents to be monitored in
 73 unprecedented detail (e.g., Hughes Clarke, 2016; Azpiroz-Zabala et al., 2017; Hage et al., 2018; Paull
 74 et al., 2018). Monterey Canyon, offshore central California (Figure 1A), has been a focus of geologic,
 75 oceanographic, and ecologic submarine canyon studies (e.g., Matos et al., 2018), making it an
 76 important analog for other submarine canyons and turbidity currents. Specifically, Monterey Canyon
 77 studies have made significant progress measuring processes and resulting deposits of sediment
 78 density flows (e.g., Paull et al., 2003, 2005, 2010, 2011, 2018; Smith et al., 2005, 2007; Xu et al.,
 79 2004, 2008, 2013, 2014; Xu and Noble, 2004; Stevens et al., 2014; Symons et al., 2017; Paull et al.,

80 2018). Sediment density flows travel down Monterey Canyon along the axial channel, over time
81 accumulating the vast Monterey submarine fan hundreds of kilometers from the canyon (e.g., Fildani
82 and Normark, 2004). Frequent (sub-annual) sediment density flow events in Monterey Canyon have
83 been sufficiently powerful to produce geomorphic change of bedforms in the canyon head and axial
84 channel (e.g., Xu et al., 2008, 2014; Smith et al., 2005, 2007; Paull et al., 2010, 2011, 2018),
85 although these recent flows did not continue far enough down-canyon to deposit sand on Monterey
86 Fan (e.g., Stevens et al., 2014). In Monterey Canyon, internal tidal flows also transport fine-grained
87 sediment between sediment density flow events (Xu and Noble, 2009).

88 Sediment enters Monterey Canyon primarily where the canyon head is incised nearly to the shoreline
89 and receives sediment from littoral cells fed largely by the Salinas, Pajaro, and San Lorenzo rivers, as
90 well as coastal cliff erosion around Monterey Bay (e.g., Griggs and Hein, 1980; Inman and Jenkins,
91 1999; Farnsworth and Warrick, 2007). Erosion and failure of the submarine canyon walls and floor
92 also contribute sediment to the axial channel (e.g., Maier et al., 2016, 2018; Paull et al., 2018).
93 Frequent sediment density flow events along the axial channel deposit coarse-grained sand and
94 bedrock clasts up to cobble size that are commonly overlain by woody plant material and a thin (few
95 cm) layer of mud at the seafloor (Paull et al., 2005, 2010). Variations in stratigraphy occur along the
96 canyon axis within tens of meters and across axial channel bedforms (Paull et al., 2010).

97 Recent studies in Monterey Canyon have demonstrated the utility of sediment traps on oceanographic
98 moorings to obtain samples of sediment directly from the water column during sediment density flow
99 events (e.g., Xu et al., 2014; Symons et al., 2017). However, a persistent challenge has been sampling
100 from the lower, powerful and destructive parts of the flow events. Xu et al. (2014) primarily
101 recovered very fine sand and silt from sediment density flow events in traps at 70–300 meters above
102 the seafloor (masf) on three moorings. Symons et al. (2017) noted that sediment in traps deployed at
103 70 masf on three moorings anchored at 820–1445 m water depth along Monterey Canyon axial
104 channel were broadly comparable to grain sizes sampled later along canyon flanks approximately 70
105 meters above the axial channel.

106 To measure sediment density flows in a comprehensive manner, a multi-institution experiment,
107 referred to as the Coordinated Canyon Experiment (CCE), was undertaken in Monterey Canyon
108 (Paull et al., 2018). The CCE included a mooring array with an unprecedented number of sediment
109 traps deployed closer to the seabed (~10 masf) than previous experiments (Table 1), and these
110 sediment traps were paired with velocity measurements and seabed samples (Fig. 1), providing a
111 unique opportunity for comparisons herein. During the 18-month-long experiment, 15 sediment
112 density flow events were measured (Paull et al., 2018). Three of these events (January 15, 2016;
113 September 1, 2016; February 3, 2017) traversed >50 km down-canyon, and others (e.g., January 22,
114 2017) only passed through part of the CCE array (Figure 1A) (Paull et al., 2018). Events comprised a
115 dense near-bed layer and an overriding, more dilute sediment cloud (Paull et al., 2018). These
116 powerful events moved down-canyon at speeds up to 7.2 m/s but were not linked to obvious or major
117 external triggers (e.g., floods, storms, earthquakes; Paull et al., 2018).

118 **1.1 Aims**

119 The overarching aim of this study is to test the fidelity of the depositional record of turbidity currents
120 (i.e., how well flows are recorded by their deposits), by comparing measurements of flow velocities,
121 sediment captured in traps within the flow, and seabed deposits. Here, we present and compare new
122 results from sediment trap samples and seafloor cores acquired during the CCE, with flow
123 measurements made over the same time interval (Paull et al., 2018). We aim to use the unique

124 observational CCE dataset to consider these questions – (1) Are flow variations faithfully recorded at
 125 a single location? We address this question at single mooring locations in two parts by considering
 126 whether trends in flow velocity over time are shown by patterns of vertical grading within samples,
 127 and whether vertical variations in flow velocity are represented by vertical grain size fractionation.
 128 (2) Are flow variations recorded along the canyon? We address this question by comparing measured
 129 velocities with grain size samples along 50-km of the canyon. (3) Do seabed deposits record grain
 130 sizes that were suspended during flow events? We compare grain sizes within trap samples with
 131 grain sizes in seabed deposits remaining after a flow event (and before the next flow event).

132

133 2 Methods

134 This study focuses on samples obtained from sediment density flow events during the CCE (Figure
 135 1A) and subsequent post-event sampling of seafloor deposits (Figure 1B, C). The CCE captured
 136 sediment density flow events in Anderson-type sediment traps deployed on six moorings along 50
 137 km of Monterey Canyon axial channel (Paull et al., 2018). Sediment traps were suspended
 138 approximately 10 masf on each mooring, with additional traps at 35–300 masf (Table 1; Figure 2A).
 139 The 18-month-long CCE was conducted in three six-month deployments (I: October 2015 – April
 140 2016; II: April – October 2016; III: October 2016 – April 2017).

141 Sediment enters Anderson-type sediment traps (after Anderson, 1977; Rendigs et al., 2009) through
 142 an open top, baffled funnel (~95–110 cm long, ~25 cm diameter (0.05 m²) top opening) and
 143 accumulates below in a clear plastic liner tube inside a PVC tube (up to ~110 cm long) (Figure 2B).
 144 To deter bioturbation in the sediment trap, the trap was initially filled with a dilute hypersaline
 145 solution of sodium azide (<5%) (e.g., Hedges et al., 1993). Intervalometers (after Rendigs et al.,
 146 2009) in Anderson sediment trap funnels dropped up to 20 discs into the liner tube at pre-set intervals
 147 (typically 8 days).

148 Sediment trap liner tubes were logged using a multi-sensor core logger (MSCL) and x-ray computed
 149 tomography (CT). CT scanning used a GE LightSpeed Ultra instrument at a Stanford University
 150 Petroleum Research Institute (SUPRI-A) Enhanced Oil Recovery and Unconventional Resources
 151 laboratory facility, at 120 kV and 140 mA with 1.25 mm axial slices (Deployment I), and a General
 152 Electric LightSpeed 16 CT scanner at the Lawrence Berkeley National Laboratory Rock Dynamic
 153 and Imaging Lab at 120 kV and 160 mA reconstructed to 0.625 mm axial slices (deployments II and
 154 III). MSCL logging included gamma-ray density, p-wave velocity, and magnetic susceptibility at the
 155 U.S. Geological Survey in Santa Cruz, California. After scanning, sediment from liner tubes were
 156 extruded in 1-cm intervals, and sub-samples were stored in Whirl-Pak plastic bags.

157 The Monterey Bay Aquarium Research Institute's (MBARI) remotely operated vehicle (ROV) *Doc*
 158 *Ricketts* collected two sets of pushcore samples (<22 cm) (after Paull et al., 2014) near the CCE
 159 mooring MS7 that were analyzed for grain size in the same lab as the sediment trap samples.
 160 Pushcores were extruded en masse or in 1-cm slices onboard the R/V *Western Flyer*. Precise timing
 161 of sediment density flow events determined by CCE instruments (Paull et al., 2018) constrains that
 162 the January 15, 2016, event was the most recent event preceding DR835 sampling in April 2016, and
 163 likewise, September 1, 2016, event was the most recent event preceding DR896 sampling in October
 164 2016.

165 Grain size was measured using a laser particle size analyzer for sediment trap samples (every 1 or 5
 166 cm) and ROV pushcore samples (every cm or selected intervals) at the National Oceanography

167 Centre, Southampton using a Malvern II Mastersizer instrument measuring in quarter-phi bins. Prior
 168 to grain size analyses, samples were sieved to remove particles >2 mm diameter, and ~ 1 cm³ sub-
 169 samples were treated with 10% sodiumhexametaphosphate solution for a total of 20 mL. Treated
 170 samples were continuously agitated on a mechanical shaker for >12 hours. Analyses were primarily
 171 run using the Malvern II autosampler, and random samples were selected and measured manually for
 172 comparison. Reported values were averaged from three runs per sample. Representative grain-size
 173 analyses presented herein are preferentially selected from near the base of an event unit to consider
 174 the coarsest sediment transported by the flow and to reduce signals from interactions with post-event
 175 internal tide flow. Representative grain-size analyses were also preferentially selected from trap liner
 176 tubes rather than funnel samples, where available and not altered by extrusion deformation (see
 177 below), for consistency in sample collection.

178 CCE moorings with sediment traps also included downward-looking 300 kHz acoustic Doppler
 179 current profilers (ADCPs) at 65 masf that measured velocity in 7-ping ensembles every 30 seconds in
 180 1-m bins between the ADCP and the seafloor (Paull et al., 2018). Herein, we use maximum ADCP-
 181 measured velocities from the entire ADCP profile during events, as well as transit velocities
 182 calculated from arrival times at successive moorings, as reported in Paull et al. (2018). For further
 183 comparison with sediment trap samples, velocities (magnitude of root mean square E-W and N-S
 184 velocities) are extracted at 10 masf (bin 055; approximately adjacent to the sediment trap samples at
 185 10 masf) during the January 15 and September 1, 2016 events. ADCP data are not presented from the
 186 January 15, 2016 event at MS1, because the MS1 mooring was transported and ripped off its anchor
 187 during the event (Paull et al., 2018). ADCP data are also not presented from the September 1, 2016
 188 event at MS4, where the ADCP malfunctioned.

189

190 **3 Results**

191 **3.1 Sediment traps**

192 Sand layers were identified visually, in CT scan images, and in grain size analyses from 21
 193 Anderson-type sediment trap deployments during the CCE (Table 1; Figure 3). Sand layers up to 60
 194 cm thick (e.g., Figure 4A) are present in the sediment trap liner tubes, and commonly overfilled the
 195 traps into the funnels in moorings MS1 to MS4 (Figures 3, S1, S2, S3). In CT scans of trap tubes,
 196 sands are lighter color and have sharp base contacts with the darker color underlying mud, wherein
 197 the transition to sand occurs over <1 cm (Figures 3, 4). Deformation along the boundary between
 198 sand and mud units is apparent in CT scans of sediment trap tubes (e.g., Figures 3A, 4A). This
 199 deformation is associated with differential loading which produced diapiric penetration of underlying
 200 muds into the overlying sand and was observed to continue during extrusion.

201 Sand units in sediment traps correspond with sediment density flow events identified with
 202 instruments (Paull et al., 2018). The coarsest sand in each event unit (fine to very coarse-grained
 203 sand) typically occurs at or near the base of the sand unit, and fines upward slightly for 1–60 cm
 204 (Figures 3 – 5; Table S1). The sand often has a unimodal distribution centered ~ 200 microns (i.e.,
 205 fine sand) (Figures 4, 5). Some samples contain a silt component and (or) a coarse-grained sand size
 206 component. The silt component may have been introduced during sample extrusion, in which
 207 previously flat sand-mud contacts were deformed and subsequent 1-cm sub-samples contained part of
 208 each unit (Figures 3, 4). In MS7 traps at 10 masf and MS5 traps at 74 masf, the sandy event unit is
 209 typically overlain by 5–10 cm (and up to ~ 30 cm) of alternating thin (<1 cm) very fine to fine sand or
 210 silt layers and mud (e.g., Figures 3, 4), which appear related to the underlying sandy event unit (see

211 section 4.1.1 for further discussion).

212 Where two traps were recovered from the same mooring, finer grain sizes and thinner sandy event
 213 units were consistently noted to occur in the upper trap compared to the lower trap (Figure 4). For
 214 example, dual traps on MS5 during each of the sediment density flow events that passed MS5 (Table
 215 1) show a decrease in the 90th percentile (d_{0.9}) grain size with increasing height above the seafloor
 216 (Figure 4E). These traps also contain larger median grain size in the lower trap compared with the
 217 upper trap (Table S1), although most of the subsamples have similar shaped grain-size distributions
 218 (Figure 4A, C).

219 Fine to medium-grained sand occurs in event units throughout the array (Figure 5). In few samples,
 220 an additional, coarser peak centered at ~1250 microns, is also observed (e.g., MS1 and MS7 in Figure
 221 5B). The averaged median grain size of sand sampled from the January 15, 2016 and September 1,
 222 2016 events at ~10 masf are comparable along 50 km of Monterey Canyon axial channel (Table S1).
 223 Median grain sizes sampled in ~10 masf traps during the January 15, 2016 event range from 297
 224 microns at MS2 to 226 microns at MS7. Median grain sizes sampled in ~10 masf traps during the
 225 September 1, 2016 event are coarsest at MS1 (432 microns), decrease at MS3 (36 microns), increase
 226 at MS4 and MS5 (182 and 259 microns, respectively), and decrease at MS7 (121 microns). The 90th
 227 percentile grain size (d_{0.9}) of September 1, 2016 event samples also show this down-canyon
 228 variation, decreasing from MS1 to MS3, increasing to MS4 and MS5, and decreasing to MS7 (Table
 229 S1).

230 3.2 ADCP-measured flow velocities and comparison to sediment traps

231 During the January 15 and September 1, 2016 events, maximum ADCP-measured velocities at
 232 mooring sites and transit velocities between moorings (as reported in Paull et al., 2018), were more
 233 than twice as fast at MS1 compared to MS7, and generally faster in the shallower (<1000 mwd)
 234 compared to the deeper end of the array (Table 2). Down-canyon decreases in this maximum ADCP-
 235 measured velocity do not correspond clearly or consistently with along-canyon variations in trap
 236 sample grain sizes (Figure 5). Although the trap at 10 masf was ripped from MS1 during the January
 237 15, 2016 event, comparable grain size distributions were sampled in traps at 10 masf across the
 238 remainder of the array, instead of a clear fining down-canyon trend, or distinctly larger grain sizes in
 239 MS2 and MS3 compared to MS5 and MS7 (Figure 5A).

240 Maximum ADCP-measured velocities at approximately 10 masf (i.e., adjacent to sediment trap
 241 samples) vary along the canyon during the January 15 and September 1, 2016 events (1.3–3.8 m/s:
 242 January 15; 0.8–4.0 m/s: Sept. 1) (Table 2; Figure 6). These velocities were greater during the
 243 January 15, 2016 event than during the September 1, 2016 event, except as measured at MS3. Very
 244 coarse grain-size sand populations in MS5 (Figure 5A) occur with the greatest ADCP-measured
 245 maximum velocities (3.8 m/s) at 10 masf from the January 15, 2016 event (Figure 6A, G). However,
 246 3.8 m/s maximum flow velocity was also measured during the January 15, 2016 event at MS2, where
 247 a similar very coarse sand population was not sampled (Figure 6A, D).

248 ADCP-measured velocities at approximately 10 masf generally are highest at the beginning of the
 249 event or increase within the initial 5–10 minutes. After 1–2 hours, velocities are <1 m/s (Figure 6).
 250 These gradually return to velocities on the order of tens of cm/s associated with internal tides (e.g.,
 251 Figure 7).

252 3.3 Post-event sampling from the seafloor

253 ROV pushcore samples acquired following the January 15 and September 1, 2016 events (and before
 254 the next event occurred) near MS7 (Table 3; Figure 1B, C), include grain sizes up to gravel and
 255 frequently medium to coarse-grained sand (Figures 8, 9). Recovery ranged from 1–23 cm during
 256 ROV *Doc Ricketts* dive number 835 (DR835) after the January 15, 2016 event, with three cores <5
 257 cm. No cores <5 cm were recovered during DR896 sampling following the September 1, 2016 event.

258 Most of the pushcores contain at least one sand layer overlain by a thin (<1 cm to 3 cm thick) mud
 259 layer (e.g., Figure 8A, B, C). Woody plant material is most common within 1 cm of the seafloor (e.g.,
 260 Figure 8F). The averaged median grain size of pushcore analyses is fine sand (155 microns) (Table
 261 S2). Medium grain size sand is common throughout (average $d_{0.9} = 403$ microns), and very coarse
 262 sand is identified in layers of some pushcores, particularly from DR835 acquired following the
 263 January 15, 2016 event (Figure 8). Both DR835 PsC-77 and DR835 PsC-69 show a slightly coarser
 264 grain-size distribution in the top centimeter (Figure 8A, B). Median grain sizes in sandy pushcore
 265 layers are up to 767 microns, but mostly less than 400 microns. Likewise, 90th percentile of these
 266 same sandy samples is mostly 250–400 microns, but nine samples have $d_{0.9} > 1000$ microns (Table
 267 S2).

268 Substantial variations in grain size distributions and stratigraphy are observed within pushcores (e.g.,
 269 Figure 8) and between closely spaced pushcores <100 m apart (Figures 1B, 1C). For example, at least
 270 two layers with coarse to very coarse sand are present within DR835 PsC-69 (Figure 8A), while a
 271 single 22-cm-thick layer of fine and medium sand is observed in nearby DR835 PsC-77 (Figure 8B).
 272 Likewise, macroscopic woody plant material is present in DR896 PsC-46 (Figure 8F) but not <200 m
 273 down-canyon in DR896 PsC-52 (Figure 8C). Lithologic heterogeneity is also observed on the
 274 seafloor, where the high-definition ROV camera shows sub-meter lateral variation (Figure 9).

275 3.4 Comparisons of trap and core samples

276 Sediment trap samples from the January 15 and September 1, 2016 events are compared to pushcores
 277 of seabed deposits sampled following each event, and before the subsequent event (Figure 1B, C).
 278 Targeted ROV pushcore samples of seabed deposits are concentrated at the distal end of the array, so
 279 we compare with MS7 sediment trap samples from approximately 10 masf for deployments I and II,
 280 respectively.

281 Grain size distributions from the January 15, 2016 event show both similarities and differences
 282 between trap and pushcore samples (Figure 10). Sand (peak centered ~200 microns) occurs in both
 283 the trap and pushcores. Pushcore samples contain muddy layers (smaller median sizes and
 284 distributions skewed towards silt) that resemble the upper part of events in trap samples (Figure
 285 10B). Some sandy layers in pushcores contain larger grain sizes (peak ~1250-1500 microns) (Figures
 286 8A, 10C) that are not present consistently in the trap samples.

287 In comparison to the January 15, 2016 event, grain size distributions for the September 1, 2016 event
 288 appear more similar between traps and cores (Figure 11B). All samples have a comparable sand peak
 289 at ~200 microns, and most samples have a minor silt peak. MS7 trap and two pushcores have samples
 290 with an additional coarse sand peak ~1250 microns.

291

292 4 Discussion

293 Turbidity current velocity measurements, samples from the water column, and seabed deposits
 294 presented in this study provide a unique opportunity to link flow processes with sediment transport
 295 and resulting deposits. We consider these questions: (1) Are flow variations faithfully recorded at a
 296 single location? (2) Are flow variations faithfully recorded along the canyon? (3) Do seabed deposits
 297 record grain sizes suspended during flow events?

298 **4.1 Are flow variations faithfully recorded at a single location?**

299 **4.1.1 Are trends in flow velocity over time shown by patterns of vertical grading within** 300 **samples?**

301 Phases of decreasing ADCP-measured flow velocity over time at approximately 10 masf during each
 302 event (e.g., Figure 6) could result in upward decreases in grain sizes of sediments from each event.
 303 Normally graded sediment trap event units (e.g., Figures 3–5, 10B) and some seabed deposits from
 304 events in this study (e.g., Figure 8) may reflect waning and thinning flows. Normally graded deposits
 305 are common in Monterey Canyon floor (e.g., Paull et al, 2005) and may record a common waning
 306 flow structure over time.

307 Above sandy event units in sediment trap tubes, slightly coarser-grained pulses of very fine-grained
 308 sand and silt likely result from sediment in the turbulent plume that either remained suspended in the
 309 water column following sediment density flow events, or were resuspended into the water column
 310 shortly after the events by internal tides (Figure 7) (e.g., Xu and Noble, 2009). If some of this fine-
 311 grained (silt-dominated) sediment settled out of the plume during periods of lower flow velocities
 312 when internal tides switched between up- and down-canyon orientations, this unconsolidated, fine-
 313 grained sand and silt could have been easily eroded and resuspended during internal tide velocities
 314 that frequently exceeded 50 cm/s (e.g., Figure 7) (Xu and Noble, 2009).

315 Sources of uncertainty in linking sediment trap samples with measurements of flow velocity and
 316 seabed deposits include exactly how and when sediment entered the traps from high-velocity flows
 317 (e.g., Symons et al., 2017). Although the moorings were designed for traps to be at 10 masf when
 318 moorings were upright, pressure records from ADCPs deployed on moorings at 65 masf show that
 319 the entire mooring string is pulled downward during the flow events (Paull et al., 2018). Presumably
 320 sediment traps tilted as they were pulled closer to the seafloor (<10 masf) during sediment density
 321 flow events, but the angles of tilt, precise height of the traps, and effect on sediment collection
 322 efficiency during the events cannot be confidently constrained from ADCP pressure or inclination
 323 records 55 m above the traps. Traps likely moved away from the seafloor as the mooring
 324 straightened, sampling from successively higher portions of the flow with time and possibly
 325 contributing to the observed normal grading in trap samples. Traps likely collected sediment most
 326 efficiently when upright in the water column, and normal grading may be enhanced by faster settling
 327 of larger grains into the trap tubes. The lack of abrasion on the outside of recovered sediment traps
 328 suggests that the recovered traps were not primarily scraping sediment from the seafloor and did not
 329 encounter the coarsest parts of the dense remobilized layer (up to ~2.5 m thick after Paull et al.,
 330 2018). However, traps that were ripped off the moorings, may have.

331 **4.1.2 Are vertical variations in flow velocity represented by vertical grain size fractionation?**

332 Traps deployed at different heights above the seafloor on the same mooring suggest that sediment
 333 density flows contained smaller grain size sediment with increasing height above the seafloor (e.g.,
 334 Figure 4), and were possibly stratified. For example, at MS5, 90th percentile sand grain size (e.g.,
 335 d_{0.9}) decreased with increasing height above the seafloor (Figure 4E). This may be a record of
 336 sediment that was lofted tens of meters above the seafloor during sediment density flow events, as

337 imaged in expanding high backscatter in both the January 15, and September 1, 2016 events (Paull et
 338 al., 2018). Similar lofting of sediment into turbulent plumes was interpreted from previous sampling
 339 of Monterey Canyon turbidity currents by Xu et al. (2014). Additionally, the upper sediment trap
 340 could have been pulled closer to the seafloor, particularly during initial high-velocity parts of the
 341 events, allowing the upper trap to sample coarser grain sizes than ever reached 74 masf (e.g., Symons
 342 et al., 2017).

343 An additional source of uncertainty includes which phases of the sediment density flow events were
 344 sampled by sediment traps. The sediment traps may not sample efficiently (e.g., Gardner, 1985), or at
 345 all, during the early, fastest phases of flow events when moorings may have been highly tilted
 346 downstream. Traps may preferentially sample from collapsing portions of the flow events when they
 347 likely returned to a more upright position, and thus, trap event layers could appear more stratified and
 348 normally graded than earlier portions of the flow event. Herein, samples from sediment traps are
 349 considered as near seafloor (<10 masf) samples from sediment density flow events and are used
 350 comparatively to discuss along-canyon trends and comparison to seafloor samples.

351

352 **4.2 Are flow variations recorded along the canyon?**

353 Sand grain sizes in traps along 50 km of the axial channel do not clearly reflect the variations in
 354 maximum ADCP-measured flow velocities nor transit velocities presented in Paull et al. (2018)
 355 (Table 2). Neither do sand grain sizes in sediment traps clearly reflect down-canyon variations in
 356 maximum ADCP-measured velocities adjacent to the sediment trap samples (~10 masf; Figure 6C–
 357 H). Sediment trap samples from the January 15 and September 1, 2016 events have similar sharp
 358 basal contacts and normal grading along 50 km down-canyon (Figures 3, 4). Grain size distributions
 359 are also rather similar along the array during individual events (Figure 5), considering that maximum
 360 ADCP-measured velocities from approximately 10 masf (near the height of the traps) vary down-
 361 canyon on the order of meters per second (Figure 6A–B). Likewise, the presence, or absence, of
 362 coarser sand populations in the sediment trap samples does not clearly reflect these variations in flow
 363 velocity measurements along the canyon. Apparent differences in grain-size populations between
 364 sediment traps, specifically the presence of coarse sand peaks (Figure 5), may be related to the
 365 complex canyon-floor morphology and down-canyon changes in slope and confinement (Figure 1;
 366 Paull et al., 2011, 2018), variations in velocities during the events (e.g., Figure 6; Paull et al., 2018),
 367 other aspects of flow velocities not captured in these measurements, and (or) erosion and deposition
 368 along the canyon axial channel (Paull et al., 2018).

369

370 **4.3 Do seabed deposits record grain sizes suspended during flow events?**

371 Comparisons of trap and seabed samples suggest that the deposit remaining on the seafloor
 372 immediately following a sediment density flow event provides a faithful record of the sand that was
 373 suspended by that flow. Coarse sand, gravel, and organic material in seafloor samples are not
 374 consistently present in sediment traps, further suggesting stratified flows. Conversely, fine-grained
 375 silty sediment in traps transported in both events and internal tidal flows (e.g., Xu and Noble, 2009)
 376 is less prevalent in seafloor deposits than traps.

377 We argue that trap samples are representative of sediment transported in the water column during an
 378 event. Owing to the lack of abrasion and tool marks on the sediment traps and other instruments on

379 the same mooring, it is unlikely that mooring sediment traps scooped sediment directly from the
380 seafloor during powerful sediment density flow events, although this possibility cannot be
381 completely eliminated. Although traps may have sampled from the collapsing portions of the flow
382 events, these stages are likely most closely related to seabed deposits, particularly in the upper
383 reaches of the canyon. Comparing sediment suspended in the water column during events and seabed
384 deposits following flow events is important, particularly because much of our knowledge of sediment
385 density flow events has been derived largely from their remaining deposits (e.g., Talling et al., 2015;
386 Covault et al., 2016; Hodgson et al., 2018).

387 Both sediment traps and pushcores contain sand (peak centered ~200 microns), but the seafloor
388 deposits variably also contain additional coarse- to very coarse-grained sand and gravel (Figure 8–
389 11). Greater variability is apparent between pushcore samples and MS7 trap samples from the
390 January 15, 2016 event compared to the September 1, 2016 event, possibly owing to the slight
391 difference in location between these two sample sets (Figure 1B, C). Larger grain-size populations in
392 seabed cores, but not trap samples, may also be related to (1) baffles on traps that would have
393 prevented large particles in the water column from entering the sediment trap, (2) velocity gradients
394 and flow stratification that may have restricted large particles in flows to levels below the height of
395 sediment traps, (3) large particles that may have moved primarily below traps as bedload, and (or) (4)
396 large clasts that may represent winnowed deposits remaining where sand may have been removed
397 during the event. Maximum ADCP-measured flow velocities and transit velocities reported in Paull
398 et al. (2018) for the January 15, 2016 event (Table 2) may have been sufficient to transport some of
399 these large particles below trap height during the event.

400 Our results highlight additional complexity in comparing sediment from flows and seafloor deposits,
401 even when contemporaneous samples are available. For example, seafloor heterogeneity, reworking
402 of seafloor sediments, and flow bypass may all lead to individual pushcores that are not fully
403 representative of the preceding flow. Heterogeneity observed on the seafloor (Figure 9) and between
404 pushcores (Figure 8) suggests that single events may generate deposits with different grain-size
405 distributions. The differences in grain size populations and stratigraphy between closely-spaced
406 pushcore samples in this study may be related to migration or modification of crescent-shaped
407 bedforms on the canyon floor (Figure 1B, C) (Paull et al., 2010). These bedforms are prevalent in
408 other canyons and channels, where they may generate similar small-scale heterogeneity and
409 stratigraphic incompleteness (e.g., Normark et al., 2009; Symons et al., 2016; Hage et al., 2018;
410 Vendettuoli et al., 2019). Seafloor heterogeneity could also result from reworking of existing
411 deposits, including erosion and deposition with bedform migration, that could mix deposits of
412 sediment transported in different flows. Erosion and deposition of Monterey Canyon axial channel
413 floor occurred during individual sediment density flow events measured in the CCE, as noted by
414 geomorphic change in the axial channel on the order of meters, bedform modification, and dense
415 remobilized layers in flow events (e.g., Paull et al., 2018). Bypass of parts of event flows may also
416 account for some variability in grain-size distributions and apparent thickness between trap and
417 pushcore samples, although neither sampling method is likely to have captured the entire event unit.

418 Identifying such reworking or bypass is complicated by the visually apparent similarity between the
419 two sets of pushcores in this and previous Monterey Canyon studies. For example, grain sizes are
420 comparable between sediment traps at approximately 10 masf along the canyon axis in this study and
421 visual descriptions of previously acquired pushcore samples from benches and canyon walls
422 approximately 10 meters above the adjacent axial channel (e.g., Paull et al., 2005, 2010; Symons et
423 al., 2017). These similarities may suggest some consistency in sediment density flow processes and
424 sediment recycling, making this study of modern processes in Monterey Canyon a relevant analog for

425 older deposits and flows that continued farther towards the fan.

426 Macroscopic woody organic material in pushcores (e.g., Figure 8F) has been noted in Monterey
 427 Canyon in the last stages of the event deposits during previous sampling studies (e.g., Paull et al.,
 428 2005), but macroscopic organics were not observed in sediment trap samples from this study. These
 429 two possibilities should be considered: (1) It remains possible that, despite the baffles, turbulence
 430 around the traps and (or) the hypersaline solution in the traps, may have prevented small (<~2 cm)
 431 macroscopic organic material from entering the trap (e.g., Fawcett et al., 2018); however, this fails to
 432 explain apparent preferential exclusion of organic matter compared to fine-grained sediment that
 433 accumulated in the traps (e.g., Figures 3, 8); (2) Alternatively, organic material may be transported
 434 near the seafloor and below the trap height.

435 Fine-grained sediment in the traps (e.g., Figure 3) is underrepresented in axial channel deposits (e.g.,
 436 Figure 8; Paull et al., 2005, 2010). At most, thin (cm-scale) mud layers are present above or between
 437 sand layers in pushcores (e.g., Figure 8). Over short timeframes, seafloor deposits appear to record
 438 sand transported during sediment density flow events, but may fail to clearly record other sediment
 439 and organic matter transport processes in the water column and along the seafloor.

440

441 **5 Conclusions**

442 This study presents a rare dataset of numerous samples from, and measurements of, sediment density
 443 flow events (commonly referred to as turbidity currents) in a submarine canyon. Comparisons of
 444 sediment trap grain sizes, seabed deposits, and flow velocity measurements from the same events
 445 show the degree to which deposits represent flow events. Thus, this study links direct measurements
 446 from powerful flows, samples of sediment suspended within flows from near the seafloor (~10 masf),
 447 and resulting seabed deposits, which has been a persistent challenge in sedimentary research. The
 448 unique dataset from the proximal 50 km along Monterey Canyon may serve as a useful analog for or
 449 comparison with sediment transport extending hundreds of kilometers farther onto Monterey Fan,
 450 occurring in other submarine canyons, modelled in future studies, and observed in ancient deposits.

451 Normal grading in sediment trap event units, as well as some seabed deposits, appears to reflect
 452 temporal waning of velocities, and thinning and collapsing of flows. Sediment density flows vary in
 453 grain size with height above the seafloor, with coarse sediment concentrated towards the seafloor and
 454 possible stratification. Sand suspended near the seafloor (~10 masf) during sediment density flow
 455 events was similar along 50 km of Monterey Canyon axial channel, suggesting some consistency in
 456 sediment transport throughout long-run-out flows measured in this study. Variations in maximum
 457 velocities measured along the canyon within sediment density flow events are not reflected clearly or
 458 consistently in sediment samples from the same flows. Although comparing trap and seafloor
 459 samples is complicated by vertical variation in the water column and seafloor heterogeneity, sand
 460 transported within the water column during events appears to be faithfully recorded in seabed
 461 deposits following two well-documented events. Conversely, fine-grained sediment transported
 462 during events and internal tidal flows that is less prevalent, and coarse sand and gravel that are
 463 observed more frequently, on the seafloor compared to traps may reflect flow stratification, transport
 464 as bedload or in a near-seafloor dense layer, and bedform migration not recorded in suspended
 465 sediment sampled in traps.

466 **6 Conflict of Interest**

467 The authors declare that the research was conducted in the absence of any commercial or financial
468 relationships that could be construed as a potential conflict of interest.

469 7 Author Contributions

470 All authors contributed to the design and implementation of the Monterey Coordinated Canyon
471 Experiment, sample acquisition and processing, and (or) development of the manuscript.

472 8 Funding

473 Funding was provided by the David and Lucile Packard Foundation, Natural Environment Research
474 Council (grant NE/K011480/1), U.S. Geological Survey (USGS) Coastal and Marine Program, and
475 Ocean University of China. Additional funding for MAC was provided by NERC National Capability
476 CLASS programme (Climate Linked Atlantic Sector Science Programme).

477 9 Acknowledgements

478 Special thanks to the USGS Marine Facilities team, especially Cordell Johnson, Dan Powers, Joanne
479 Ferreira, Rob Wyland, Tim Elfers, Pete Dal Ferro, and Jenny White, for operation of sediment traps
480 and upper canyon moorings; Ashley Tuton and University of Southampton for grain size analyses;
481 Sharon Borglin and Tim Kneafsey at the Lawrence Berkeley National Laboratory Rock Dynamic and
482 Imaging Lab, and Elliot Kim and Anthony Kovscek at the SUPRI-A Laboratory; Mike Torresan and
483 PCMSC Sediment Laboratories; MBARI's ship crews, ROV pilots, and CCE shipboard scientific
484 parties.

485

486 References

- 487 Anderson, R.Y. (1977). Short term sedimentation response in lakes in western United States as
488 measured by automated sampling. *Limnol. Oceanogr.* 22, 423–433.
- 489 Anderson, K.S., Graham, S.A. and Hubbard, S.M. (2006). Facies, architecture, and origin of a
490 reservoir-scale sand-rich succession within submarine canyon fill: Insights from Wagon Caves Rock
491 (Paleocene), Santa Lucia Range, California, U.S.A. *J. Sed. Res.* 76, 819–838. doi:
492 10.2110/jsr.2006.066
- 493 Azpiroz-Zabala, M., Cartigny, M.J.B., Talling, P.J., Parsons, D.R., Sumner, E.J., Clare, M.A., et al.
494 (2017). Newly recognized turbidity current structure can explain prolonged flushing of submarine
495 canyons. *Sci. Adv.* 3, e1700200. doi: 10.1126/sciadv.1700200
- 496 Clare, M.A., Vardy, M.E., Cartigny, M.J.B., Talling, P.J., Himsforth, M.D., Dix, J.K., et al. (2017). Direct monitoring of active
497 geohazards: Emerging geophysical tools for deep-water assessments. *Near Surf. Geophys.* 15, 427–
498 444. doi: 10.3997/1873-0604.2017033
- 499 Cronin, B.T. and Kidd, R.B. (1998). Heterogeneity and lithotype distribution in ancient deep-sea
500 canyons: Point Lobos deep-sea canyon as a reservoir analogue. *Sed. Geol.* 115, 315–349.
- 501 Farnsworth, K.L. and Warrick, J.A. (2007). Sources, dispersal, and fate of fine sediment supplied to
502 coastal California. *U.S. Geolog. Surv. Sci. Investigation Report 2007-5254*, 77 p.

- 503 Fawcett, S.E., Johnson, K.S., Riser, S., Van Oostende, N., and Sigman, D.M. (2018). Low-nutrient
 504 organic matter in the Sargasso Sea thermocline: A hypothesis for its role, identity, and carbon cycle
 505 implications. *Mar. Chem.* doi: 10.1016/j.marchem.2018.10.008
 506 (2004). A simple universal equation for grain settling velocity. *J. Sed. Res.* 74, 933–937.
- 507 Ferreira, J.T., Rosenberger, K.J., Maier, K.L., 2019, Time-series oceanographic data from the
 508 Monterey Canyon, CA October 2015 – March 2017. U.S. Geological Survey,
 509 <https://doi.org/10.5066/F7FT8J7Q>.
- 510 Fildani, A., Normark, W.R., 2004. Late Quaternary evolution of channel and lobe complexes of
 511 Monterey Fan. *Mar. Geol.* 206, 199–223. doi: 10.1016/j.margeo.2004.03.001.
- 512 Gardner, W.D., 1985. The effect of tilt on sediment trap efficiency. *Deep-Sea Res.* 32, 349–361.
- 513 Griggs, G.B. and Hein, J.R. (1980). Sources, dispersal, and clay mineral composition of fine-grained
 514 sediment off central and northern California. *J. Geology* 88, 541–566.
- 515 Hage, S., Cartigny, M.J.B., Clare, M.A., Sumner, E.J., Vendettuloi, D., Hughes Clarke, J.E., et al.
 516 (2018). How to recognize crescentic bedforms formed by supercritical turbidity currents in the
 517 geologic record: Insights from active submarine channels. *Geology* 46, 563–566. doi:
 518 10.1130/G40095.1
- 519 Harris, P.T. and Whiteway, T. (2011). Global distribution of large submarine canyons: Geomorphic
 520 differences between active and passive continental margins. *Mar. Geol.* 285, 69–86. doi:
 521 10.1016/j.margeo.2011.05.008
- 522 Hedges, J.I., Lee, C., Wakeham, S.G., Hernes, P.J. and Peterson, M.L. (1993). Effects of poisons and
 523 preservatives on the fluxes and elemental compositions of sediment trap materials. *J. Mar. Res.* 51,
 524 651–668.
- 525 Hodgson, D.M., Bernhard, A., Clare, M.A., Da Silva, A.-C., Fosdick, J.E., Mauz, B., et al. (2018).
 526 Grand challenges (and great opportunities) in sedimentology, stratigraphy, and diagenesis research.
 527 *Front. Earth Sci.* 6:173. doi: 10.3389/feart.2018.00173
- 528 Hughes Clarke, J.E. (2016). First wide-angle view of channelized turbidity currents links migrating
 529 cyclic steps to flow characteristics. *Nat. Comm.* 7, 11986. doi: 10.1038/ncomms11896
- 530 Inman, D.L. and Jenkins, S.A. (1999). Climate change and the episodicity of sediment flux of small
 531 California rivers. *J. Geology* 107, 251–270.
- 532 Komar, P.D. (1985). The hydraulic interpretation of turbidites from their grain sizes and sedimentary
 533 structures. *Sedimentology* 32, 395–407.
- 534 Liu, J.T., Hsu, R.T., Hung, J.-J., Chang, Y.-P., Wang, Y.-H., Rendle-Bühring, R.H., et al. (2016).
 535 From the highest to the deepest: The Gaoping River – Gaoping Submarine Canyon dispersal system.
 536 *Earth-Sci. Rev.* 153, 274–300. doi: 10.1016/j.earscirev.2015.10.012
- 537 Maier, K.L., Hartwell, S.R., Johnson, S.Y., Davenport, C. and Greene, H.G. (2016). Offshore and
 538 onshore geology and geomorphology, Monterey Canyon and Vicinity map area, California, *sheet 10*
 539 in Dartnell, P., Maier, K.L., Erdey, M.D., Dieter, B.E., Golden, N.E., Johnson, S.Y., et al. (P.

- 540 Dartnell and S.A. Cochran, eds.), California State Waters Map Series—Monterey Canyon and
541 Vicinity. U.S. Geol. Surv. Open-File Report 2016-1072, 85 p., 10 sheets, scale 1:24,000. doi:
542 10.3133/ofr20161072
- 543 Maier, K.L., Johnson, S.Y. and Hart, P. (2018). Controls on submarine canyon head evolution,
544 migration, and fill in Monterey Bay, offshore central California. *Mar. Geol.* 404, 24–40. doi:
545 10.1016/j.margeo.2018.06.014
- 546 Matos, F.L., Ross, S.W., Huvenne, V.A.I., Davies, J.S. and Cunha, M.R. (2018). Canyons pride and
547 prejudice: Exploring the submarine canyon research landscape, a history of geographic and thematic
548 bias. *Progr. Oceanogr.* doi: 10.1016/j.pocean.2018.04.010
- 549 Mutti, E. and Normark, W.R. (1987). “Comparing examples of modern and ancient turbidite systems:
550 problems and concepts,” in *Marine Clastic Sedimentology: Concepts and Case Studies*, eds J.K.
551 Leggett and G.G. Zuffa (London: Graham and Trotman), 1–38.
- 552 Normark, W.R. (1974). “Submarine canyons and fan valleys: Factors affecting growth patterns of
553 deep-sea fans,” in *Modern and ancient geosynclinals sedimentation*, eds R.H. Dott and R. Shaver.
554 *Society of Economic Paleontologists and Mineralogists Special Publication* 19, 56–68. doi:
555 10.2110/pec.74.19.0056
- 556 Normark, W.R., Paull, C.K., Caress, D.W., Ussler, W. III and Sliter, R. (2009). Fine-scale relief
557 related to Late Holocene channel shifting within the floor of the upper Redondo Fan, offshore
558 Southern California. *Sedimentology* 56, 1690–1704. doi: 10.1111/j.1365-3091.2009.10152.x
- 559 Paull, C.K., Ussler, W. III, Greene, H.G., Keaten, R., Mitts, P. and Barry, J. (2003). Caught in the
560 act: The 20 December 2001 gravity flow event in Monterey Canyon. *Geo-Ma. Lett.* 22, 227–232. doi:
561 10.1007/s00367-003-0117-2
- 562 Paull, C.K., Mitts, P., Ussler, W. III, Keaten, R. and Greene, H.G. (2005). Trail of sand in upper
563 Monterey Canyon: Offshore California. *Geol. Soc. Am. Bull.* 117, 1134–1145. doi:
564 10.1130/B25390.1
- 565 Paull, C.K., Ussler, W. III, Caress, D.W., Lundsten, E., Covault, J.A., Maier, K.L., et al. (2010).
566 Origins of large crescent-shaped bedforms within the axial channel of Monterey Canyon, offshore
567 California. *Geosphere* 6, 1–20. doi: 10.1130/GES00527.1
- 568 Paull, C.K., Caress, D.W., Ussler, W. III, Lundsten, E. and Meiner-Johnson, M. (2011). High-
569 resolution bathymetry of the axial channels within Monterey and Soquel submarine canyons,
570 offshore central California. *Geosphere* 7, 1077–1101. doi: 10.1130/GES00636.1
- 571 Paull, C.K., McGann, M., Sumner, E.J., Barnes, P.M., Lundsten, E.M., Anderson, K., et al. (2014).
572 Sub-decadal turbidite frequency during the early Holocene: Eel Fan, offshore northern California.
573 *Geology* 42, 855–858, doi: 10.1130/G35768.1
- 574 Paull, C.K., Talling, P.J., Maier, K.L., Parsons, D., Xu, J., Caress, D.W., Gwiazda, R., et al. (2018).
575 Powerful turbidity currents driven by dense basal layers. *Nat. Commun.* 9, 4114. doi:
576 10.1038/s41467-018-06254-6

- 577 Rendigs, R.R., Anderson, R.Y., Xu, J., Davis, R.E. and Bergeron, E. (2009). The partition
 578 intervalometer: A programmable underwater timer for marking accumulated sediment profiles
 579 collected in Anderson sediment traps: Development, operation, testing procedures, and field results.
 580 *U.S. Geol. Surv. Open-File Report 2009-1101*. <https://pubs.usgs.gov/of/2009/1101>
- 581 Shepard, F.P. (1951). Mass movements in submarine canyon heads. *Trans., Am. Geophys. Un.* 32,
 582 405–418.
- 583 Smith, D.P., Ruiz, G., Kvitek, R. and Iampietro, P.J. (2005). Semiannual patterns of erosion and
 584 deposition in upper Monterey Canyon from serial multibeam bathymetry. *Geol. Soc. Am. Bull.* 117,
 585 1123–1133. doi: 10.1130/B25510.1
- 586 Smith, D.P., Kvitek, R., Iampietro, P.J. and Wong, K. (2007). Twenty-nine months of geomorphic
 587 change in upper Monterey Canyon (2002–2005). *Mar. Geol.* 236, 79–94. doi:
 588 10.1016/j.margeo.2006.09.024
- 589 Stevens, T., Paull, C.K., Ussler, W. III, McGann, M., Buylaert, J.-P. and Lundsten, E. (2014). The
 590 timing of sediment transport down Monterey Submarine Canyon, offshore California. *Geol. Soc. Am.*
 591 *Bull.* 126, 103–121. doi: 10.1130/B30931.1
- 592 Symons, W.O., Sumner, E.J., Talling, P.J., Cartigny, M.J.B. and Clare, M.A. (2016). Large-scale
 593 sediment waves and scours on the modern seafloor and their implications for the prevalence of
 594 supercritical flows. *Mar. Geol.* 371, 130–148. doi: 10.1016/j.margeo.2015.11.009
- 595 Symons, W.O., Sumner, E.J., Paull, C.K., Cartigny, M.J.B., Xu, J.P., Maier, K.L., et al. (2017). A
 596 new model for turbidity current behavior based on integration of flow monitoring and precision
 597 coring in a submarine canyon. *Geology* 45, 367–370. doi: 10.1130/G38764.1
- 598 Talling, P.J., Allin, J., Armitage, D.A., Arnott, R.W.C., Cartigny, M.J.B., Clare, M.A., et al. (2015).
 599 Key future directions for research on turbidity currents and their deposits. *J. Sed. Res.* 85, 153–169.
 600 doi: 10.2110/jsr.2015.03
- 601 Vendettuoli, D., Clare, M.A., Hughes Clarke, J.E., Vellinga, A., Hizzett, J., Hage, S., et al. (2019, in
 602 press). Daily bathymetric surveys document how stratigraphy is built and its extreme incompleteness
 603 in submarine channels. *Earth Planet. Sci. Lett.* 515, 231 – 247,
 604 <https://doi.org/10.1016/j.epsl.2019.03.033>.
- 605 Williams, T.A., Graham, S.A., and Constenius, K.N. (1998). Recognition of a Santonian submarine
 606 canyon, Great Valley Group, Sacramento Basin, California: Implications for petroleum exploration
 607 and sequence stratigraphy of deep-marine strata. *Am. Assoc. Petrol. Bull.* 82, 1575–1595.
- 608 Xu, J.P. (2011). Measuring currents in submarine canyons: Technological and scientific progress in
 609 the past 30 years. *Geosphere* 7, 868–876. doi: 10.1130/GES00640.1
- 610 Xu, J.P. and Noble, M.A. (2004). In-situ measurements of velocity structure within turbidity currents.
 611 *Geophys. Res. Lett.* 31, L09311. doi: 10.1029/2004GL019718
- 612 Xu, J.P., and Noble, M.A. (2009). Currents in Monterey Submarine Canyon. *J. Geophys. Res.* 114,
 613 C03004. doi: 10.1029/2008JC004992

- 614 Xu, J.P., Noble, M.A. and Rosenfeld, L.K. (2004). In-situ measurements of velocity structure within
615 turbidity currents. *Geophys. Res. Lett.* 31, L09311. doi: 10.1029/2004GL019718
- 616 Xu, J.P., Wong, F.L., Kvittek, R., Smith, D.P. and Paull, C.K. (2008). Sandwave migration in
617 Monterey Submarine Canyon, Central California. *Mar. Geol.* 248, 193–212. doi:
618 10.1016/j.margeo.2007.11.005
- 619 Xu, J.P., Swarzenski, P.W., Noble, M. and Li, A.-C. (2010). Event-driven sediment flux in Hueneme
620 and Mugu submarine canyons, southern California. *Mar. Geol.* 269, 74–88. doi:
621 10.1016/j.margeo.2009.12.007
- 622 Xu, J.P., Barry, J.P. and Paull, C.K. (2013). Small-scale turbidity currents in a big submarine canyon.
623 *Geology* 41, 143–146. doi: 10.1130/G33727.1
- 624 Xu, J.P., Sequeiros, O.E. and Noble, M.A. (2014). Sediment concentrations, flow conditions, and
625 downstream evolution of two turbidity currents, Monterey Canyon, USA. *Deep-Sea Res. I* 89, 11–34.
626 doi: 10.1016/j.dsr.2014.04.001

627

628 **Tables**629 **Table 1.** Anderson-type sediment trap samples.630 **Table 2.** Sediment density flow event velocities (m/s).631 **Table 3.** Remotely operated vehicle (ROV) *Doc Ricketts* pushcore samples.

632

633 **Figures**

634 **Figure 1.** Sample locations in Monterey Canyon, offshore central California. **(A)** Coordinated
635 Canyon Experiment (CCE) moorings along Monterey Canyon axial channel (modified from Paull et
636 al., 2018). Dashed arrows signify longshore transport of sand into Monterey Canyon. **(B)** Locations
637 of remotely operate vehicle (ROV) pushcores from DR835, collected April 19, 2016 and plotted on
638 Monterey Bay Aquarium Research Institute (MBARI) mapping autonomous underwater vehicle
639 (AUV) 1-m lateral resolution slope-shaded multibeam bathymetry acquired on April 18, 2016. **(C)**
640 Locations of ROV pushcores from DR896, collected October 19, 2016 and plotted on MBARI AUV
641 1-m lateral resolution slope-shaded multibeam bathymetry acquired on December 6, 2016.

642 **Figure 2.** Schematic illustrations of Coordinated Canyon Experiment moorings and sediment traps
643 deployed in Monterey Canyon. **(A)** Anderson-type sediment trap on mooring (not to scale) (modified
644 from Paull et al., 2018). ADCP: acoustic Doppler current profiler. masf: meters above the seafloor.
645 **(B)** Anderson-type sediment trap (not to scale).

646 **Figure 3.** Sediment trap sample examples. Data is shown as computed tomography (CT) images
647 (left; shading adjusted independently for each image) and grain size (right; d_{0.1} (10th percentile; red),
648 d_[4,3] (volume weighted mean; black), and d_{0.9} (90th percentile; gray)). Intervalometers in the trap
649 funnels deployed discs into the trap tubes at preset intervals during deployment; these discs are seen
650 in cross-section in the CT images and labeled with dates as numeric month and day (e.g., 1122 is
651 November 22). Sediment density flow event units contain coarser sediment (sand) and a lighter shade

652 in CT than fine-grained inter-event units. **(A)** Deployment I. Sediment units from the January 15,
 653 2016 event are highlighted in red. **(B)** Deployment III. Sediment units from the February 3, 2017 and
 654 November 24, 2016 events are highlighted in blue and green, respectively.

655 **Figure 4.** Variation between traps at different heights above the seafloor. **(A)** January 15, 2016
 656 sediment density flow event in mooring MS5 sediment traps at 11 meters above the seafloor (masf)
 657 and 74 masf. Data shown as in Figure 3 (*left*), with additional grain-size distribution profiles within
 658 the January 15, 2016 event unit (*right*). **(B)** MS5 ADCP-measured velocity at 10 masf and 64 masf
 659 from the January 15, 2016 event. **(C)** September 1, 2016 sediment density flow event in MS5
 660 sediment traps. Data shown as in Part A. **(D)** MS5 ADCP-measured velocity from the September 1,
 661 2016 event, as in Part B. **(E)** d_{0.9} grain size of coarsest extruded 1-cm samples from sediment
 662 density flow event units in MS5 sediment traps.

663 **Figure 5.** Grain-size distributions from sediment density flow event units in sediment traps. Solid
 664 lines indicate samples from traps deployed at ~10 meters above the seafloor (masf), and dashed lines
 665 indicate samples from traps deployed at >10 masf. **(A)** January 15, 2016, event. **(B)** September 1,
 666 2016 event. **(C)** February 3, 2017 event. **(D)** Stratigraphy of the September 1, 2016 event shown as
 667 grain-size distributions down-canyon (*right to left*, as in Figure 1).

668 **Figure 6.** Acoustic Doppler current profiler (ADCP)-measured velocity from approximately 10
 669 meters above the seafloor (masf; ADCP bin 055) adjacent to sediment trap samples at 10 masf. Grain
 670 size axes calculated after Komar (1985) and Ferguson and Church (2004). Velocity profiles in **(A)**
 671 from the January 15, 2016 event and **(B)** from the September 1, 2016 event, are labeled with mooring
 672 (MS#) and maximum ADCP-measured velocity (m/s) in each event at ~10 masf. Plots **(C)** through
 673 **(H)** show ADCP-measured velocities from each mooring and the range of measured d_{0.1} to d_{0.9}
 674 grain sizes in sediment traps from ~10 masf.

675 **Figure 7.** Velocity during and following the January 15, 2016 event measured at MS7. **(A)** Color-
 676 contoured ADCP velocity panel. Range (y-axis) is shown as meters below the ADCP instrument,
 677 deployed at 65 meters above the seafloor on mooring MS7. When the mooring is upright, the seafloor
 678 is at range 65 m, which is the base of this plot. **(B)** ADCP-measured velocity at approximately 10
 679 meters above the seafloor (masf) from Part A. **(C)** Color-contoured ADCP-measured velocity (labels
 680 as in Part A), showing post-event internal tide variations. **(D)** Velocity profile from approximately 10
 681 masf in Part C. **(E)** Scatter plot of MS7 velocity directions from 15 masf during Deployment I.
 682 Down-canyon internal tides and sediment density flow events are oriented primarily to the west-
 683 northwest, and up-canyon internal tides oriented primarily to the north-northeast.

684 **Figure 8.** Remotely operated vehicle (ROV) pushcore samples acquired near MS7. **(A, B)** Pushcores
 685 acquired in April 2016, following the January 15, 2016 event, shown as schematic log (*left*) and
 686 grain-size distributions (*right*). Stratigraphy and coarse grain size populations differ between these
 687 two closely spaced pushcores (57 m apart). See Figure 1B for sample locations. **(C) through (F)**
 688 Pushcores acquired in October 2016, after the September 1, 2016 event, shown as photographs and
 689 grain-size distributions. Woody plant material in sand is highlighted in Part F. See Figure 1C for
 690 sample locations.

691 **Figure 9.** Remotely operated vehicle (ROV) photographs of seafloor heterogeneity observed during
 692 pushcore sampling. **(A)** Photograph of pushcore DR835 PsC-69 from an area of sand adjacent to
 693 exposed cobbles and pebbles. **(B)** Photographs of DR896 PsC-76 acquisition at times $t_1 - t_3$. Large
 694 clasts are exposed adjacent to the pushcore (t_1), and buried pebbles fell out of the base of the
 695 pushcore (t_2 and t_3).

696 **Figure 10.** Comparison of sediment from the January 15, 2016 sediment density flow event in MS7
 697 trap and seabed samples. See Figure 1B for sample locations. **(A)** Photograph of an extruded and split

698 pushcore acquired following the January 15, 2016 event. **(B)** Stratigraphy of grain-size distributions
 699 from the January 15, 2016 event unit in MS7 sediment trap at 10 masf. **(C)** Comparison of grain-size
 700 distributions from MS7 and coarsest grain-size distributions from 1-cm extruded pushcore intervals
 701 of ROV pushcores (Table S2).

702 **Figure 11.** Comparison of sediment from the September 1, 2016 sediment density flow event in MS7
 703 trap and seabed samples. See Figure 1C for sample locations. **(A)** Photograph of an extruded and split
 704 pushcore acquired following the September 1, 2016 event. **(B)** Comparison of the coarsest grain-size
 705 distributions from MS7 sediment trap at 10 masf and nearby pushcores (Table S2).

706

707 *Supplementary Tables*

708 **Supplementary Table S1.** Grain size summary for sediment density flow events in sediment traps.

709 **Supplementary Table S2.** Grain size summary for pushcore samples.

710

711 *Supplementary Figures*

712 **Supplementary Figure S1.** Summary of Anderson sediment trap results and interpretations of
 713 sediment density flow event units from Deployment I (October 2015 – April 2016). Datum is base of
 714 trap tube sediment (i.e., start of deployment). From left to right, data shown are CT images,
 715 intervalometer disc dates (numeric month and day), and grain size measurements at 1 cm intervals,
 716 including d_{0.1} in red, d_[4,3] in black, and d_{0.9} in gray. Grain size results from bulk samples
 717 extracted from the sediment trap funnels are shown above trap tube data. Interpreted sediment from
 718 January 15, 2016 sediment density flow event is highlighted in red.

719 **Supplementary Figure S2.** Summary of Anderson sediment trap results and interpretations of
 720 sediment density flow event units from Deployment II (April 2016 – October 2016). Data shown as
 721 in Figure S1, with grain size measurements every 5 cm. Interpreted sediment from September 1, 2016
 722 sediment density flow event highlighted in green.

723 **Supplementary Figure S3.** Summary of Anderson sediment trap results and interpretations of
 724 sediment density flow event units from Deployment III (October 2016 – April 2017). Data shown as
 725 in Figure S2. Interpretation of events on November 24, 2016 and January 9, January 22, February 3,
 726 and February 18, 2017 are highlighted. For more information, see event chart in Paull et al. (2018).

727

728 **Data Availability Statement**

729 The datasets generated and analyzed in this study and the CCE can be accessed in the supplementary
 730 files, with Paull et al. (2018) at <https://doi.org/10.1594/IEDA/324529>,
 731 [https://www.mbari.org/science/seafloor-processes/geological-changes/coordinated-canyon-](https://www.mbari.org/science/seafloor-processes/geological-changes/coordinated-canyon-experiment-datareport-main-page/)
 732 [experiment-datareport-main-page/](https://www.mbari.org/science/seafloor-processes/geological-changes/coordinated-canyon-experiment-datareport-main-page/), <https://www.mbari.org/cce-instruments-2019/>, and in Ferreira et
 733 al. (2019) USGS data release at <https://doi.org/10.5066/F7FT8J7Q>.

Table 1. Anderson-type sediment trap samples.

Deployment	Trap		water depth (m)	Location		Timing			Samples		Sediment Density Flow Events ⁴
	Mooring Station	masf ¹		latitude	longitude	deployed ²	recovered ²	status at recovery	total 1-cm slices	discs	
I	MS1	10	287	36.793280	-121.844600	20151006	N/A	ripped off	N/A	N/A	N/A
I	MS1	35	287	36.793280	-121.844600	20151006	20160117	overfull	79	Yes	Jan. 15
I	MS2	10	527	36.788270	-121.903400	20151005	20160405	overfull	80	Yes	Jan. 15
I	MS3	10	831	36.764970	-121.969700	20151005	20160405	overfull	89	Yes	Jan. 15
I	MS4	10	1286	36.735795	-122.016478	20151007	20160405	overfull	95	No	Jan. 15
I	MS5	11	1449	36.714960	-122.013000	20151020	20160405	overfull	95	Yes	Jan. 15
I	MS5	74	1449	36.714960	-122.013000	20151020	20160405	overfull	91	No	Jan. 15
I	MS7	10	1849	36.701620	-122.097500	20151027	20160412	full	87	No	Jan. 15
I	MS7	300	1849	36.701620	-122.097500	20151027	20160412	underfilled	9	No	none
II	MS1	10	278	36.793240	-121.844716	20160404	20161003	overfull	93	No	Sept. 1
II	MS2	10	527	36.787832	-121.903508	20160407	20161003	overfull	95	Yes	none
II	MS3	10	822	36.764763	-121.969575	20160407	20161004	overfull	89	Yes	Sept. 1
II	MS4	10	1285	36.736000	-122.016667	20160408	20161004	overfull	97	No	Sept. 1
II	MS5	11	1445	36.715517	-122.012875	20160408	20161004	overfull	91	No	Sept. 1
II	MS5	74	1445	36.715517	-122.012875	20160408	20161004	full	74	No	Sept. 1
II	MS7	10	1849	36.701784	-122.098400	20160420	20161010	full	N/A ³	No	Sept. 1
II	MS7	300	1849	36.701784	-122.098400	20160420	20161010	underfilled	19	No	none
III	MS1	10	290	36.793557	-121.845658	20161006	20170321	full	77	Yes	Nov. 24
III	MS1	35	290	36.793557	-121.845658	20161006	20170321	underfilled	13	N/A	none
III	MS2	10	523	36.787250	-121.903383	20161006	N/A	ripped off	N/A	N/A	N/A
III	MS3	10	817	36.765045	-121.969880	20161006	20170321	overfull	96	Yes	Nov. 24 Jan. 9
III	MS3	35	817	36.765045	-121.969880	20161006	20170321	overfull	89	No	Nov. 24 Jan. 9 Feb. 3
III	MS4	10	1263	36.735898	-122.016470	20161007	20170322	overfull	80	No	Jan. 22 Feb. 3
III	MS5	11	1439	36.716333	-122.012833	20161007	20170206	overfull	87	Yes	Jan. 22 Feb. 3
III	MS5	74	1439	36.716333	-122.012833	20161007	20170206	overfull	84	No	Jan. 22 Feb. 3
III	MS7	10	1849	36.701549	-122.098372	20161019	20170404	full	67	No	Feb. 3
III	MS7	300	1849	36.701549	-122.098372	20161019	20170404	underfilled	24	No	Feb. 3

¹masf: meters above the seafloor

²dates shown as numeric year, month, day

³sample material recovered but not stratigraphy

⁴event units in sediment trap tube or funnel (see text and Paull et al., 2018)

737

738 Table 2. Sediment density flow event velocities (m/s)

Event Date	Mooring	Max ADCP-measured velocity ¹	Max ADCP-measured velocity at 10 masf ²	Transit Velocity ¹
Jan. 15, 2016	MS1	8.0	N/A	N/A
	MS2	4.2	3.8	5.8
	MS3	5.3	1.3	7.2
	MS4	2.6	2.0	6.6
	MS5	4.1	3.8	3.7
	MS7	2.6	1.9	2.5
	Sept. 1, 2016	MS1	4.0	4.0
MS2		2.6	0.8	4.0
MS3		3.7	2.4	4.4
MS4		N/A	N/A	4.8
MS5		3.6	2.8	4.8
MS7		1.0	0.7	1.5

¹from Paull et al. (2018)²bin 055; see Figure 6

739

740

741

Table 3. Remotely operated vehicle (ROV) *Doc Ricketts* pushcore samples.

Sample ID	Sample Type	Latitude	Longitude	Water Depth (m)	Acquisition Date ¹	Length (cm)
DR835 PsC-49	pushcore	36.701706	-122.093783	1836.8	20160419	1
DR835 PsC-60	pushcore	36.701663	-122.093853	1836.8	20160419	3
DR835 PsC-77	pushcore	36.701695	-122.093529	1836.7	20160419	23
DR835 PsC-80	pushcore	36.701732	-122.094100	1838.9	20160419	10
DR835 PsC-69	pushcore	36.701855	-122.094137	1838.9	20160419	12
DR835 PsC-52	pushcore	36.701719	-122.094373	1838.6	20160419	18
DR835 PsC-54	pushcore	36.701747	-122.094737	1839.9	20160419	2
DR835 PsC-50	pushcore	36.701740	-122.094741	1839.9	20160419	11
DR896 PsC-76	pushcore	36.701802	-122.093893	1837.6	20161019	8
DR896 PsC-75	pushcore	36.701708	-122.092709	1835.0	20161019	16
DR896 PsC-41	pushcore	36.701809	-122.092806	1835.0	20161019	16
DR896 PsC-49	pushcore	36.701754	-122.093541	1837.6	20161019	11
DR896 PsC-46	pushcore	36.701752	-122.093581	1837.6	20161019	7
DR896 PsC-52	pushcore	36.701679	-122.094209	1839.5	20161019	16
DR896 PsC-73	pushcore	36.701770	-122.094166	1839.5	20161019	16
DR896 PsC-55	pushcore	36.701521	-122.094837	1839.5	20161019	10
DR896 PsC-54	pushcore	36.701898	-122.094847	1840.9	20161019	5
DR896 PsC-67	pushcore	36.701790	-122.098065	1850.5	20161019	10
DR896 PsC-50	pushcore	36.701798	-122.098083	1850.5	20161019	15
DR896 PsC-48	pushcore	36.701682	-122.098710	1851.4	20161019	7
DR896 PsC-77	pushcore	36.701692	-122.098643	1851.4	20161019	7

¹date shown as numeric year month day

742

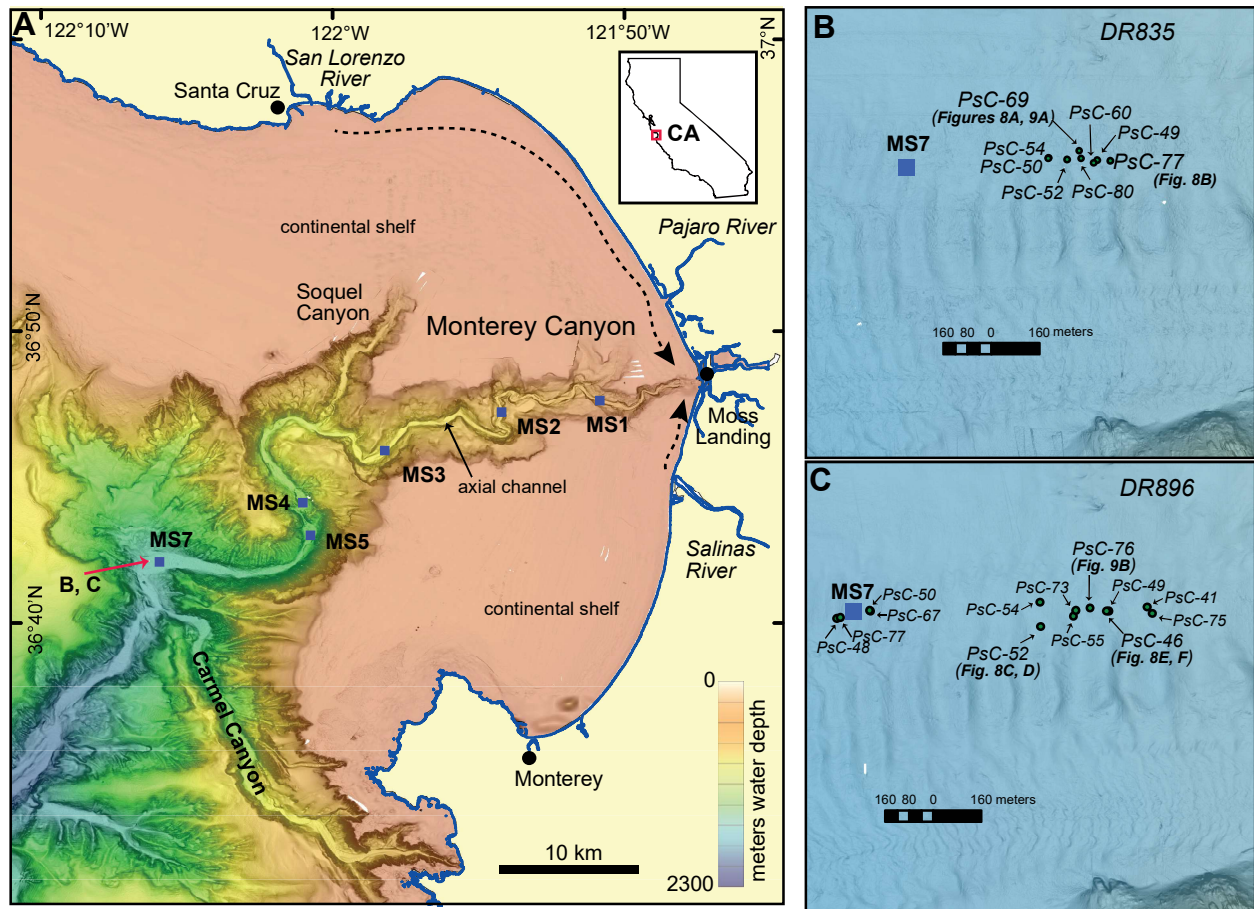


Figure 1. Sample locations in Monterey Canyon, offshore central California. (A) Coordinated Canyon Experiment (CCE) moorings along Monterey Canyon axial channel (modified from Paull et al., 2018). Dashed arrows signify longshore transport of sand into Monterey Canyon. (B) Locations of remotely operate vehicle (ROV) pushcores from DR835, collected April 19, 2016 and plotted on Monterey Bay Aquarium Research Institute (MBARI) mapping autonomous underwater vehicle (AUV) 1-m lateral resolution slope-shaded multibeam bathymetry acquired on April 18, 2016. (C) Locations of ROV pushcores from DR896, collected October 19, 2016 and plotted on MBARI AUV 1-m lateral resolution slope-shaded multibeam bathymetry acquired on December 6, 2016.

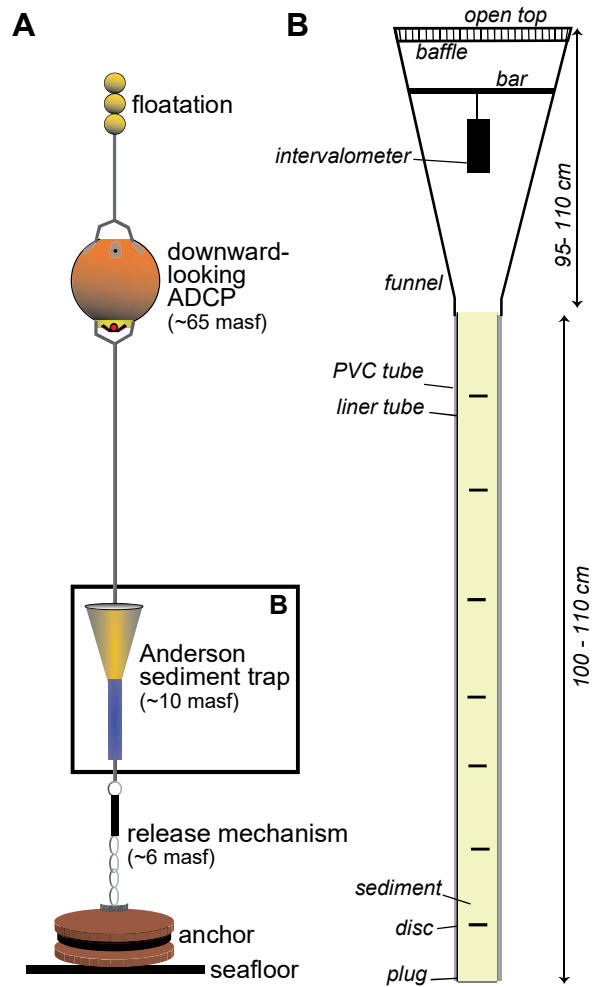


Figure 2. Schematic illustrations of Coordinated Canyon Experiment moorings and sediment traps deployed in Monterey Canyon. (A) Anderson-type sediment trap on mooring (not to scale) (modified from Paull et al., 2018). ADCP: acoustic Doppler current profiler. masf: meters above the seafloor. (B) Anderson-type sediment trap (not to scale).

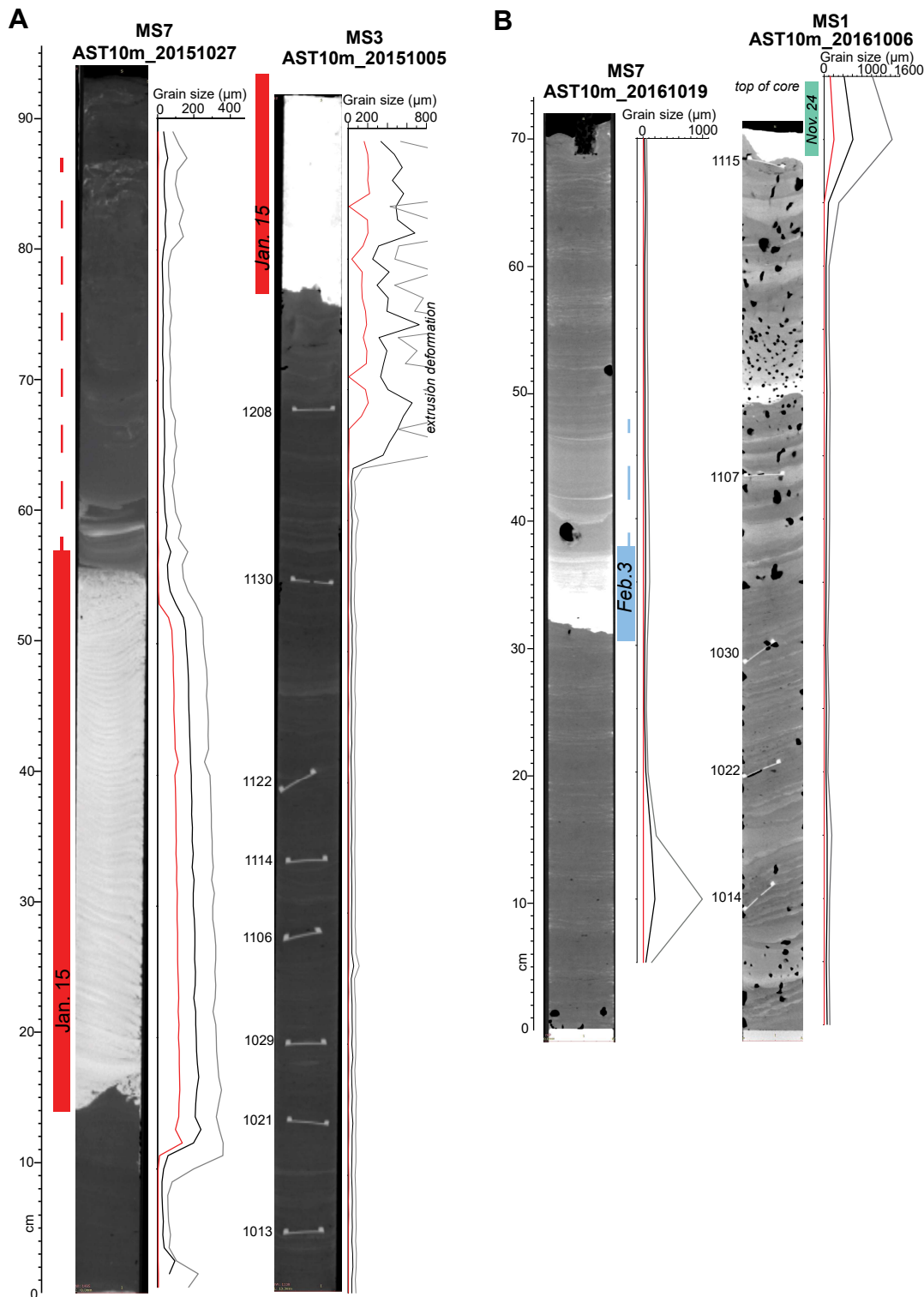


Figure 3. Sediment trap sample examples. Data is shown as computed tomography (CT) images (left; shading adjusted independently for each image) and grain size (right; $d_{0.1}$ (10th percentile; red), $d_{[4,3]}$ (volume weighted mean; black), and $d_{0.9}$ (90th percentile; gray)). Intervalometers in the trap funnels deployed discs into the trap tubes at preset intervals during deployment; these discs are seen in cross-section in the CT images and labeled with dates as numeric month and day (e.g., 1122 is November 22). Sediment density flow event units contain coarser sediment (sand) and a lighter shade in CT than fine-grained inter-event units. (A) Deployment I. Sediment units from the January 15, 2016 event are highlighted in red. (B) Deployment III. Sediment units from the February 3, 2017 and November 24, 2016 events are highlighted in blue and green, respectively.

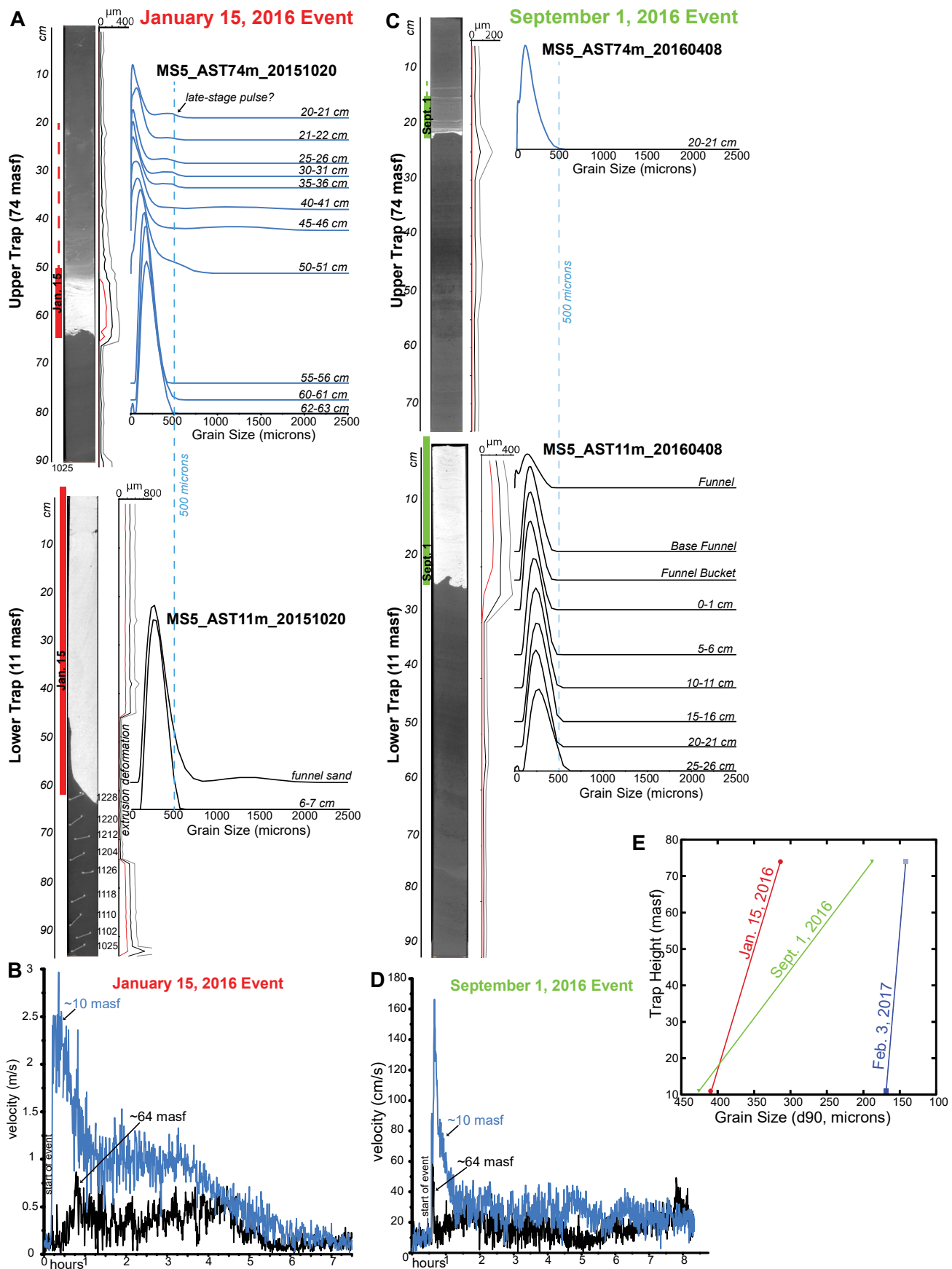


Figure 4. Variation between traps at different heights above the seafloor. (A) January 15, 2016 sediment density flow event in mooring MS5 sediment traps at 11 meters above the seafloor (masf) and 74 masf. Data shown as in Figure 3 (left), with additional grain-size distribution profiles within the January 15, 2016 event unit (right). (B) MS5 ADCP-measured velocity at 10 masf and 64 masf from the January 15, 2016 event. (C) September 1, 2016 sediment density flow event in MS5 sediment traps. Data shown as in Part A. (D) MS5 ADCP-measured velocity from the September 1, 2016 event, as in Part B. (E) d_{0.9} grain size of coarsest extruded 1-cm samples from sediment density flow event units in MS5 sediment traps.

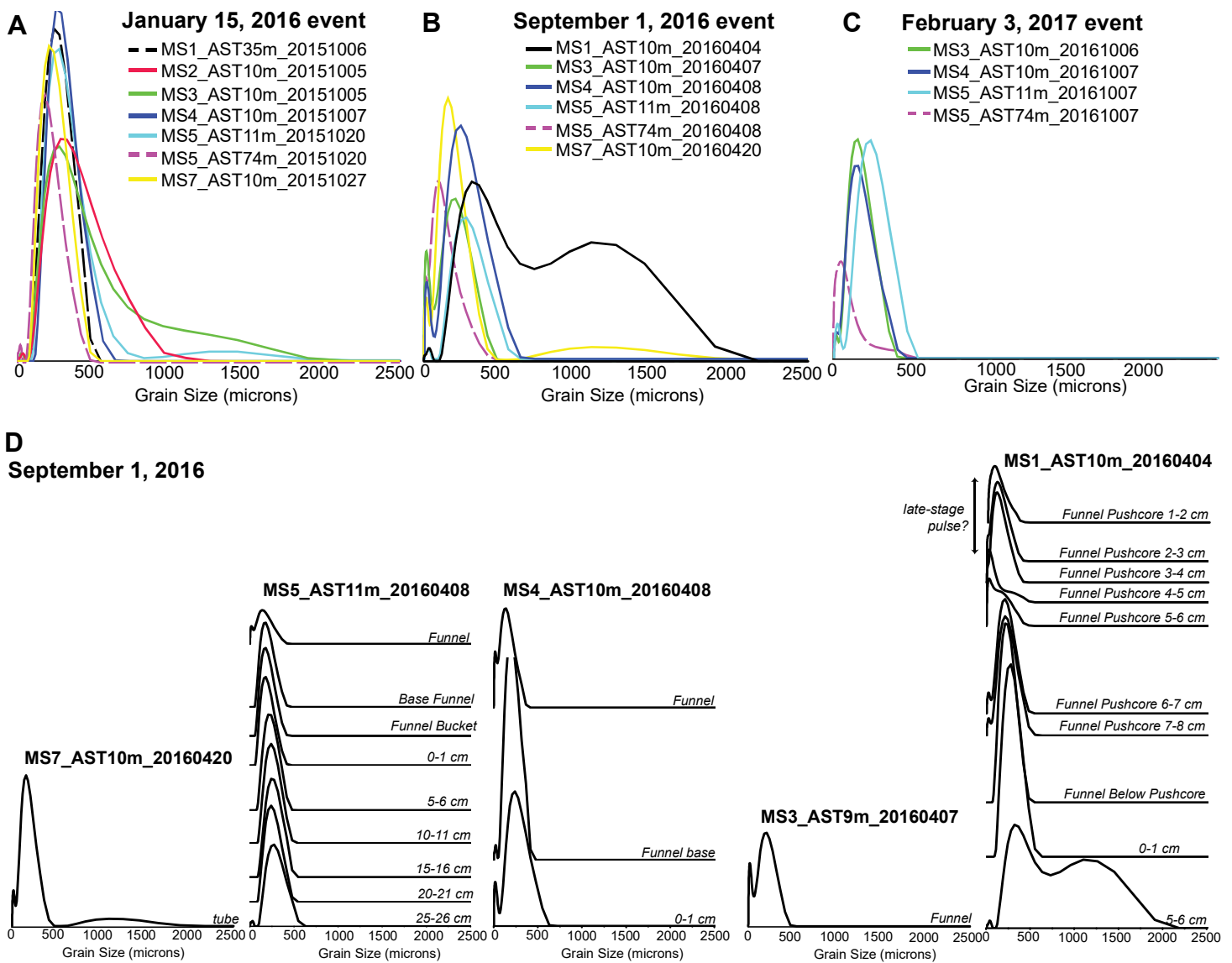


Figure 5. Grain-size distributions from sediment density flow event units in sediment traps. Solid lines indicate samples from traps deployed at ~10 meters above the seafloor (masf), and dashed lines indicate samples from traps deployed at >10 masf. (A) January 15, 2016, event. (B) September 1, 2016 event. (C) February 3, 2017 event. (D) Stratigraphy of the September 1, 2016 event shown as grain-size distributions down-canyon (right to left, as in Figure 1).

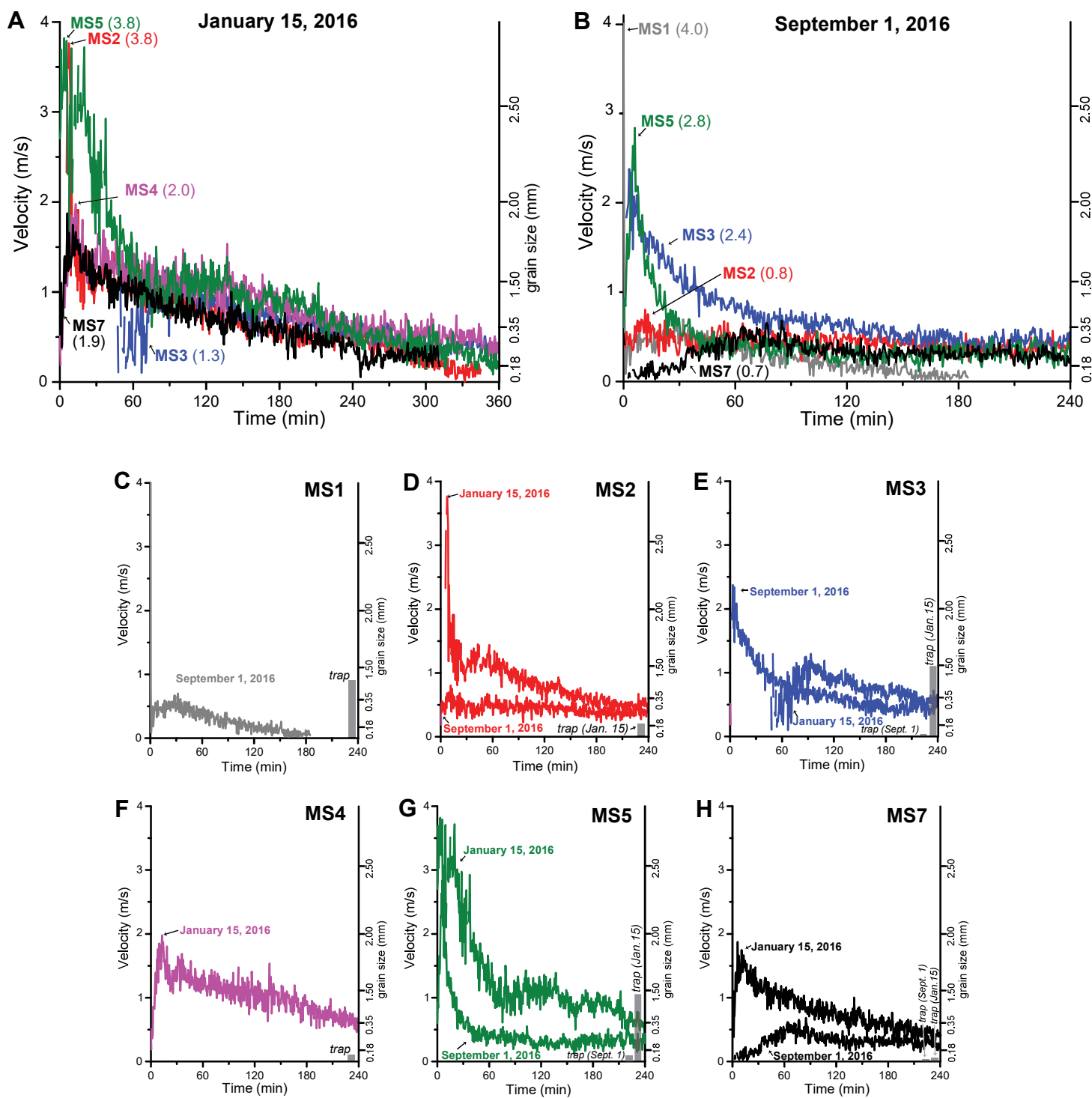


Figure 6. Acoustic Doppler current profiler (ADCP)-measured velocity from approximately 10 meters above the seafloor (masf; ADCP bin 055) adjacent to sediment trap samples at 10 masf. Grain size axes calculated after Komar (1985) and Ferguson and Church (2004). Velocity profiles in (A) from the January 15, 2016 event and (B) from the September 1, 2016 event, are labeled with mooring (MS#) and maximum ADCP-measured velocity (m/s) in each event at ~10 masf. Plots (C) through (H) show ADCP-measured velocities from each mooring and the range of measured d_{0.1} to d_{0.9} grain sizes in sediment traps from ~10 masf.

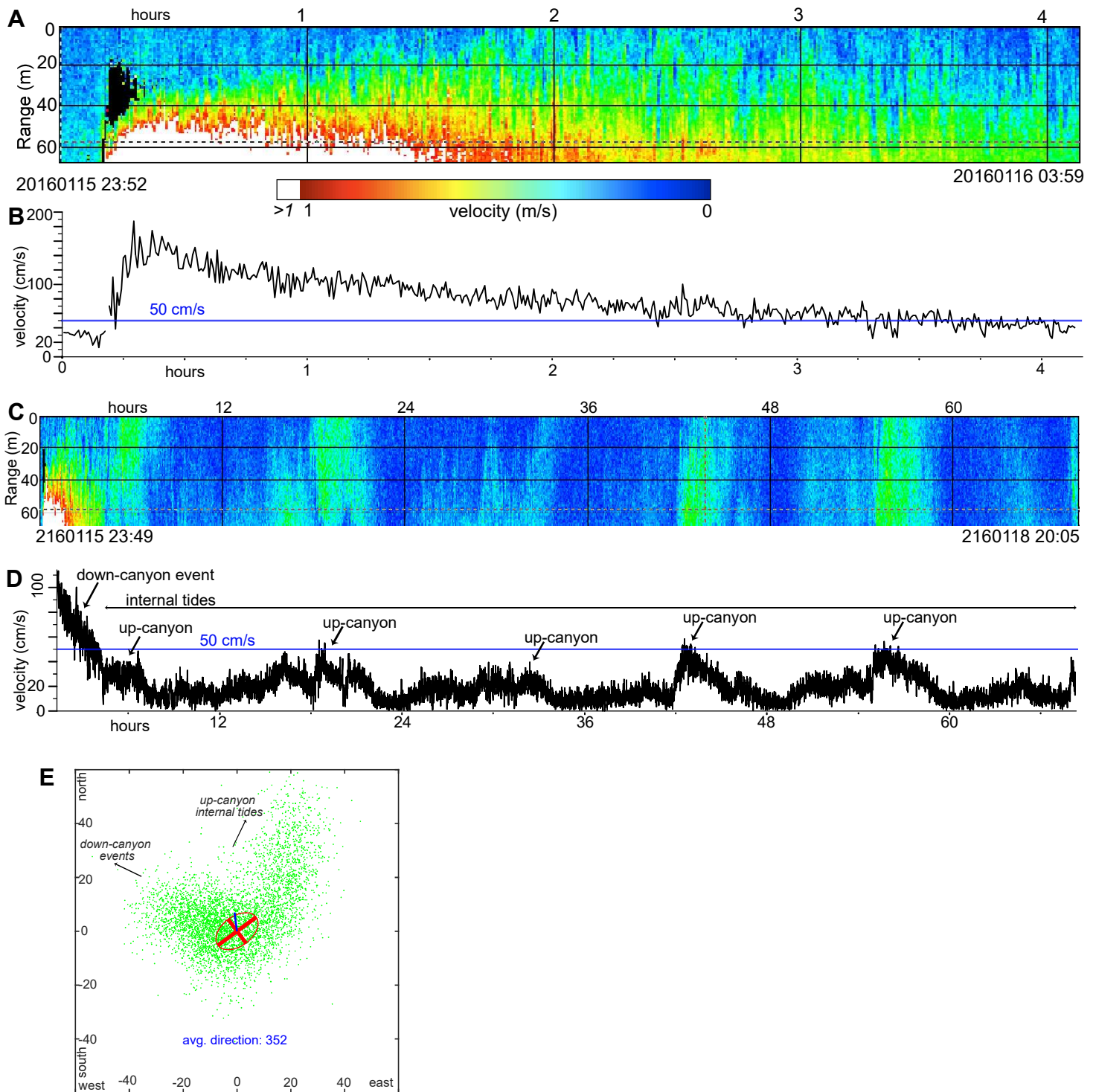


Figure 7. Velocity during and following the January 15, 2016 event measured at MS7. (A) Color-contoured ADCP velocity panel. Range (y-axis) is shown as meters below the ADCP instrument, deployed at 65 meters above the seafloor on mooring MS7. When the mooring is upright, the seafloor is at range 65 m, which is the base of this plot. (B) ADCP-measured velocity at approximately 10 meters above the seafloor (masf) from Part A. (C) Color-contoured ADCP-measured velocity (labels as in Part A), showing post-event internal tide variations. (D) Velocity profile from approximately 10 masf in Part C. (E) Scatter plot of MS7 velocity directions from 15 masf during Deployment I. Down-canyon internal tides and sediment density flow events are oriented primarily to the west-northwest, and up-canyon internal tides oriented primarily to the north-northeast.

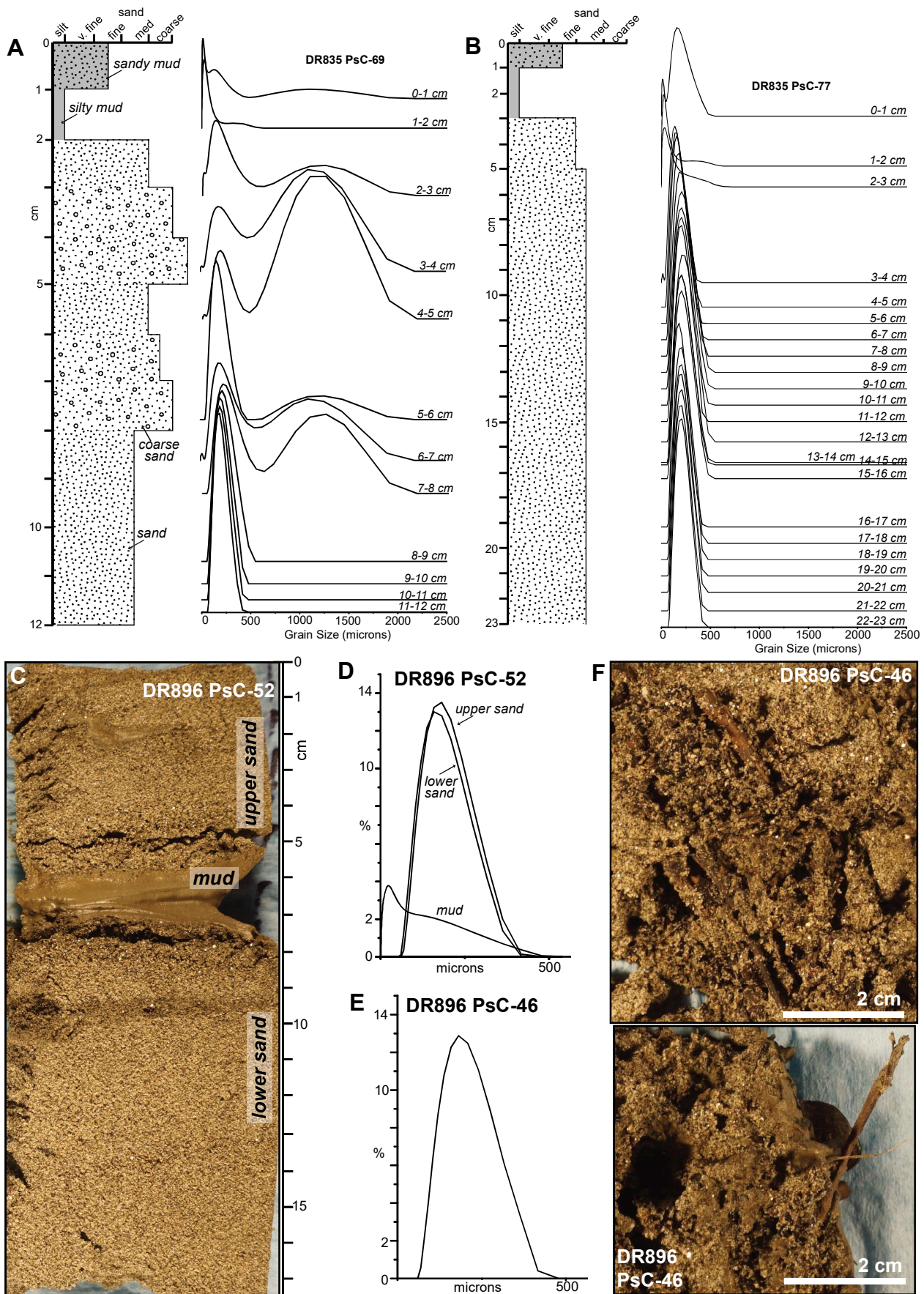


Figure 8. Remotely operated vehicle (ROV) pushcore samples acquired near MS7. (A, B) Pushcores acquired in April 2016, following the January 15, 2016 event, shown as schematic log (left) and grain-size distributions (right). Stratigraphy and coarse grain size populations differ between these two closely spaced pushcores (57 m apart). See Figure 1B for sample locations. (C) through (F) Pushcores acquired in October 2016, after the September 1, 2016 event, shown as photographs and grain-size distributions. Woody plant material in sand is highlighted in Part F. See Figure 1C for sample locations.

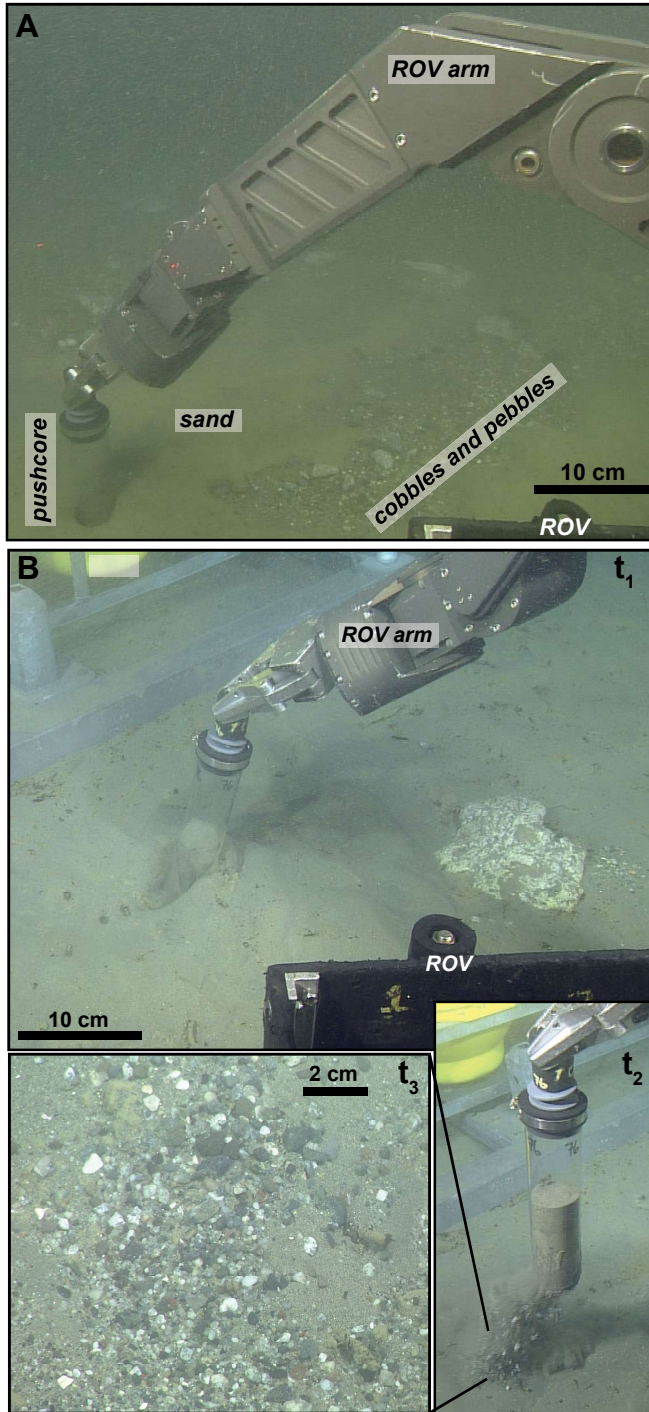


Figure 9. Remotely operated vehicle (ROV) photographs of seafloor heterogeneity observed during pushcore sampling. (A) Photograph of pushcore DR835 PsC-69 from an area of sand adjacent to exposed cobbles and pebbles. (B) Photographs of DR896 PsC-76 acquisition at times t_1 – t_3 . Large clasts are exposed adjacent to the pushcore (t_1), and buried pebbles fell out of the base of the pushcore (t_2 and t_3).

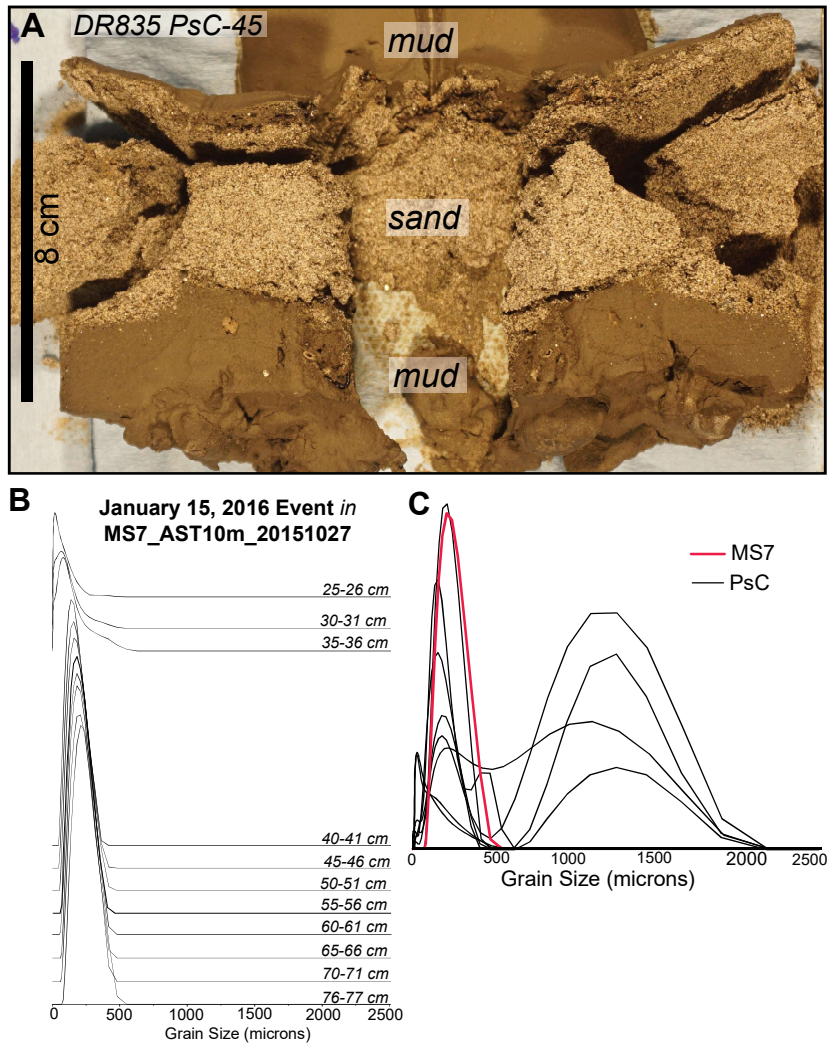


Figure 10. Comparison of sediment from the January 15, 2016 sediment density flow event in MS7 trap and seabed samples. See Figure 1B for sample locations. (A) Photograph of an extruded and split pushcore acquired following the January 15, 2016 event. (B) Stratigraphy of grain-size distributions from the January 15, 2016 event unit in MS7 sediment trap at 10 masf. (C) Comparison of grain-size distributions from MS7 and coarsest grain-size distributions from 1-cm extruded pushcore intervals of ROV pushcores (Table S2).

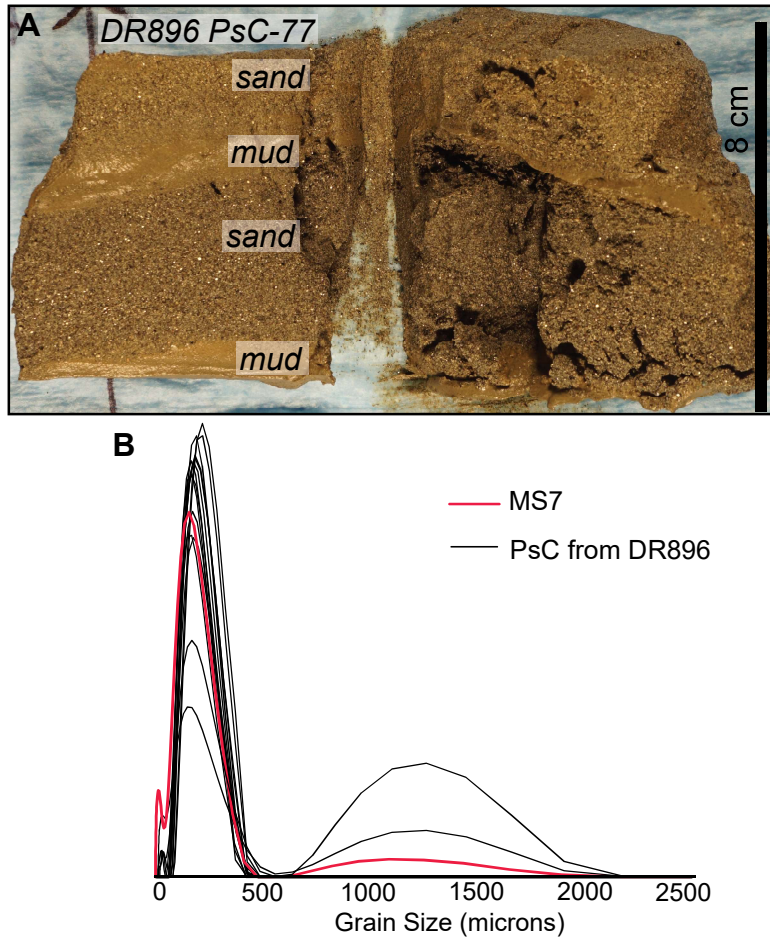


Figure 11. Comparison of sediment from the September 1, 2016 sediment density flow event in MS7 trap and seabed samples. See Figure 1C for sample locations. (A) Photograph of an extruded and split pushcore acquired following the September 1, 2016 event. (B) Comparison of the coarsest grain-size distributions from MS7 sediment trap at 10 masf and nearby pushcores (Table S2).